2024 International Materials Selection Challenge Final Reports

Developed and curated by the Ansys Academic Development Team

education@ansys.com

Ansys Software Used

This resource uses:

- Ansys Granta EduPack™ a teaching software for materials education.
- Ansys Discovery™ a 3D product simulation software.
- Ansys Mechanical™a structural finite element analysis software.
- Ansys Fluent® fluid simulation software.
- Ansys FENSAP-ICE™ in-flight aircraft icing simulation.

Summary

This resource collects the reports of the finalist projects of the 2024 Ansys International Material Selection Challenge. These projects were submitted by student teams from universities in Italy, Malta, Colombia and Brazil. Each proposal was supervised by a professor and reviewed by members of the Ansys Academic Program before being presented in front of a jury composed of Prof. Elena Maria Tejado Garrido (UPM, Spain), Sara Onrubia Garcia (Ansys Spain), Prof. Dr. André Canal Marques (UNISINOS, Brazil), Prof. Barbara Del Curto (Politecnico di Milano, Italy) and Prof. Germán Alcalá Penadés (UCM, Spain). The final presentations were held at the Moncloa Campus of the Polytechnic University of Madrid on November 6th, 2024.

The project reports collected here are meant to serve as inspiration for students and educators working on material selection projects. They demonstrate how Ansys Granta EduPack can foster innovation and optimal product designs, with examples using many of its tools as well as other Ansys simulation software.

Table of Contents

Sustainable Alternatives to Steel in Transmission Tower (Pylon) Design: Exploring the Potential of Bio-Based and Natural Fibers

Universidad Pontificia Bolivariana,Medellín, Colombia

Supervisor: Hader Vladimir Martínez Tejada

Students: Felipe Ayala Restrepo, Diego Alejandro Jimenez Areiza, and Juan José Soto Jaramillo

Report Contents

1. Summary

The increasing adoption of renewable energy sources necessitates the development of sustainable and efficient electricity transmission infrastructure. Traditional steel transmission towers, while effective, present challenges related to visual impact, environmental concerns, and resource depletion. This research investigates the potential of alternative materials, such as banana and plantain fibers, and basalt fiber, to replace steel in transmission tower construction. By utilizing Ansys Granta EduPack software, the study evaluates the mechanical-structural performance, energy consumption, and environmental impact of these materials, aiming to identify sustainable alternatives that meet the demands of modern power transmission while minimizing negative environmental effects.

2. Objectives

The primary objective of this research is to investigate and propose sustainable alternatives to steel for the construction of electricity transmission towers, with a focus on banana and plantain fibers, and basalt fiber. The study aims to achieve this through the following steps:

1. Material Screening and Selection: Utilize Ansys Granta EduPack software to conduct a comprehensive screening of potential materials based on mechanical-structural performance, energy consumption, and environmental impact. The focus will be on identifying materials that outperform traditional steel in these aspects.
2. Comparative Analysis: Conduct a detailed comparative analysis of the selected alternative materials (banana and plantain fibers, basalt fiber) against steel, considering factors such as strength, durability, cost-effectiveness, and overall sustainability.
3. Simulation and Validation: Employ simulation techniques to validate the performance of the chosen

alternative materials under realistic operating conditions, ensuring their suitability for transmission tower construction.

4. Design Optimization: Explore innovative design approaches that leverage the unique properties of the selected alternative materials to optimize the structural integrity, aesthetics, and environmental performance of transmission towers.
5. Recommendations and Implementation: Provide recommendations for the adoption and implementation of the proposed alternative materials in the construction of sustainable and aesthetically pleasing transmission towers, contributing to a greener energy infrastructure.

3. Problem statement

The growing demand for renewable energy necessitates the development of sustainable and visually appealing electricity transmission infrastructure [1]. Conventional steel transmission towers, while functional, face increasing opposition due to their negative visual impact, environmental concerns, and logistical complexities [2]. The exploration of alternative materials, particularly abundant Colombian natural fibers like hemp, bamboo, and agave, presents a promising opportunity to address these challenges [3]. However, the key challenge lies in ensuring that these natural fibers, even when combined with other materials like basalt fiber, can match the structural performance and mechanical strength of steel, while also offering advantages in terms of sustainability, aesthetics, and environmental integration [4] [5]. The exploitation of biomass resources in developed countries, including Colombia, is rapidly transforming, creating a unique opportunity to leverage these resources for sustainable infrastructure development. This research aims to rigorously evaluate the potential of Colombian natural fibers and basalt fiber as viable alternatives to steel in transmission tower construction, contributing to a more sustainable and aesthetically pleasing energy landscape.

4. Proposed solution

The primary aim of this research was to investigate whether, under the conditions experienced by a typical transmission tower, there are materials that could potentially replace steel. Could natural fibers be among these alternatives? And would they be suitable for a variety of tower geometries and heights?

To address these questions, a three-stage process was employed to construct selection charts. Initially, calculations were made to create indices based on three key material properties relevant to this application: density, Young's modulus, and yield strength. Each stage then incorporated an additional factor into the analysis: material cost, embodied energy in primary production, and CO2 footprint from primary production, as shown in equations (1) to (6).

Since the objective was to minimize these indices, the graphs were generated using Granta software. As the refinement process progressed to the third stage, the results highlighted a group of ceramics and some metals as common options. However, a zone of natural materials also emerged as a potential new solution for this application, as shown in Figures (1) and (2). These materials were proposed as a solution for a column subjected to a high load coefficient and with varying cross-sectional areas.

Building upon the solid foundation established in our previous discussion, we can further explore the potential of Colombian natural fibers as an innovative and sustainable alternative for the construction of energy transmission towers. Colombia, renowned for its rich biodiversity, boasts a vast array of natural fibers that could revolutionize the construction of these structures. Among the most promising

candidates are hemp, bamboo, and agave fibers. Hemp, besides being a source of high-strength textile fibers, possesses excellent insulating properties and can be cultivated in various Colombian climates. Bamboo, a rapidly growing grass, readily adapts to different altitudes and edaphoclimatic conditions, offering high tensile and flexural strength. Agave fibers, such as fique, have been traditionally used in the manufacture of ropes and fabrics, exhibiting excellent resistance to humidity and UV radiation.

5. Results and conclusions

As depicted in Figures (1) and (2), the primary fibers that emerged as solutions for this application are basalt, banana fiber, mica, and ramie fiber. As evident in the graphs, following a comprehensive analysis, these materials demonstrated the most favorable values, making them suitable candidates for future transmission towers and other civil engineering applications.

To complement the graphical findings, a series of simulations were conducted using Ansys software to compare the performance of a basalt fiber column against columns made of steel and concrete. The results are presented in Figures (3), (4), and (5). The parameters for all three columns were identical: 5 meters in height, a load of 100,000 N, and a diameter of 150 mm.

In conclusion, this research underscores the immense potential of natural fibers to contribute to a more sustainable society. It highlights the opportunity to transition towards solutions that not only benefit their specific field of application but also promote eco-friendly practices in the manufacturing of the objects that keep our world moving forward. Additionally, the reuse of biomass presents another promising avenue that, in conjunction with natural fibers, can help address the global waste problem.

6. References

[1] Liu, W., Misra, M., Asadi, K., & Mohanty, A. K. (2015). Sustainable natural fiber-reinforced polymer composites: Opportunities and challenges. Journal of Polymers and the Environment, 23, 338-350.

[2] Ashby, M. F. (2010). Materials selection in mechanical design. Butterworth-Heinemann.

[3] Valadez-Gonzalez, A., Cervantes-Uc, J. M., Oskoueian, F., & Herrera-Franco, P. J. (2013). Plant fiber composites: A review of recent developments. Industrial Crops and Products, 42, 291-311.

[4] Jawaid, M., & Khalil, H. P. S. A. (2011). Cellulosic/synthetic fiber reinforced polymer hybrid composites: A review. Carbohydrate polymers, 86(1), 1-18.

[5] Saba, N., & Jawaid, M. (2014). A review on potentiality of nano-filler/natural fiber reinforced polymer hybrid composites. Composites Part B: Engineering, 67, 264-276.

7. Appendix

Equations:

$$M1 = \frac{\rho * Material\ cost}{\sigma_y}\ (1),\ M2 = \frac{\rho * Material\ cost}{\sqrt{E}}\ (2),\ M3 = \frac{\rho * Embodied\ energy}{\sigma_y}\ (3),$$

$$M4 = \frac{\rho * Embodied\ energy}{\sqrt{E}}\ (4),\ M5 = \frac{\rho * CO_2 footprint}{\sigma_y}\ (5),\ M6 = \frac{\rho * CO_2 footprint}{\sqrt{E}}(6).$$

Figures:

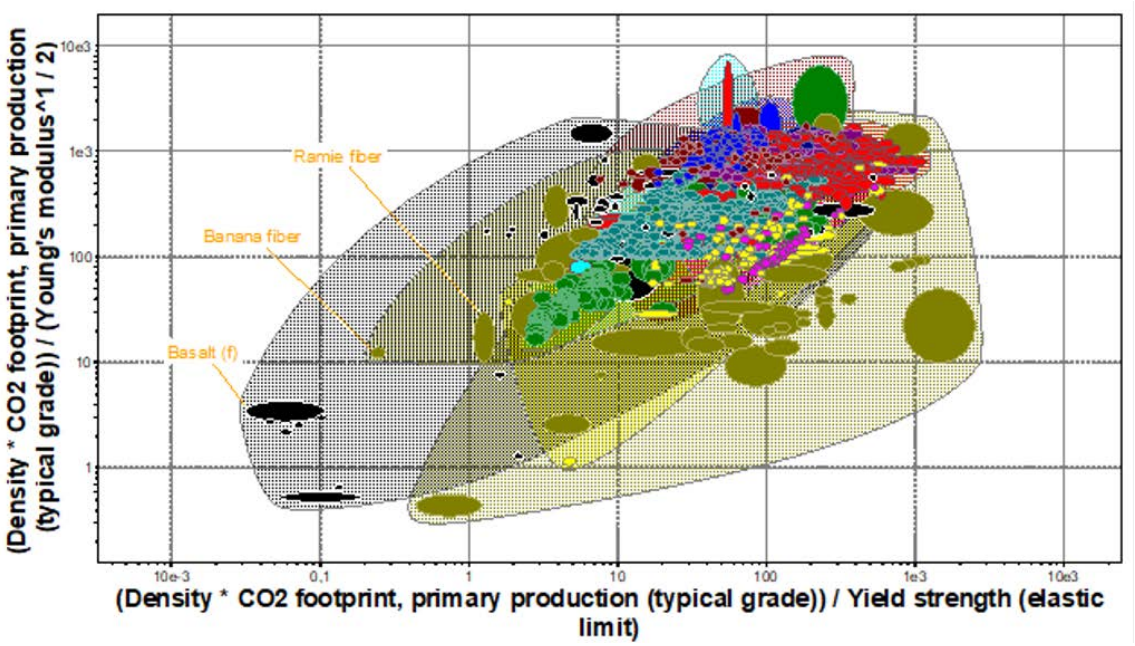

Figure 1: M5 vs M6 graph and the resultant materials that are the suggested solutions.

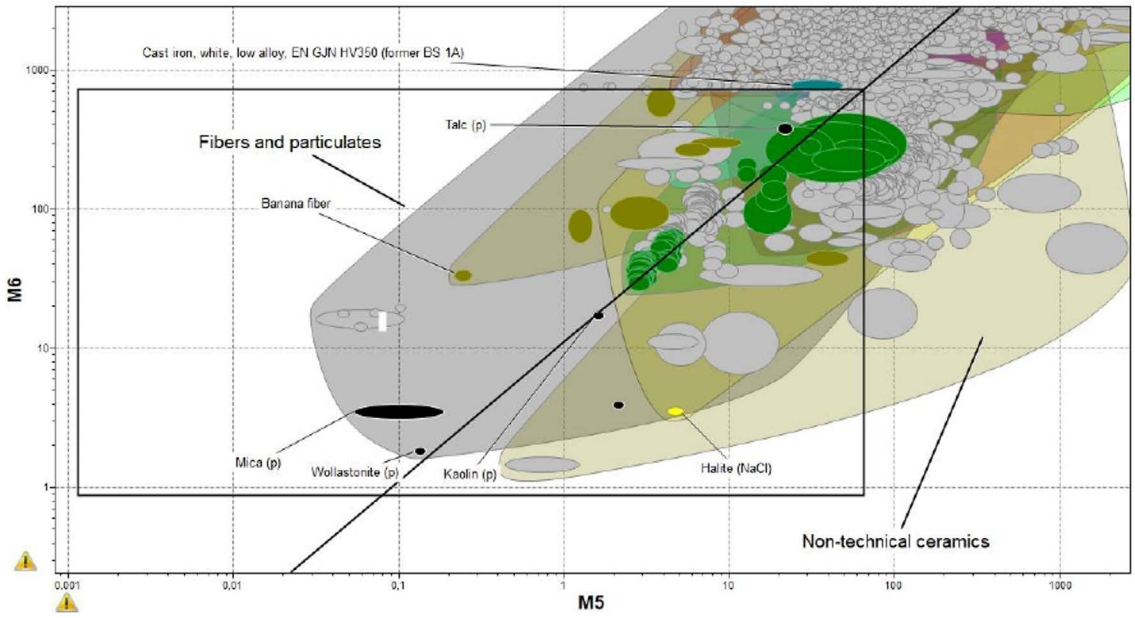

Figure 2: A more near view from the group of materials that can be the options for the transmission towers.

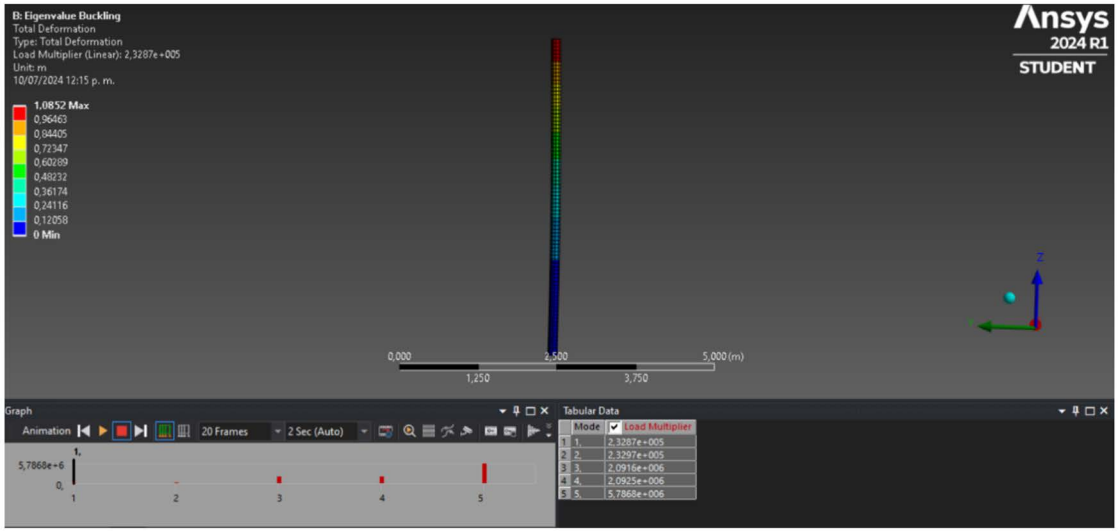

Figure 3: Basalt fiber column simulated and its results.

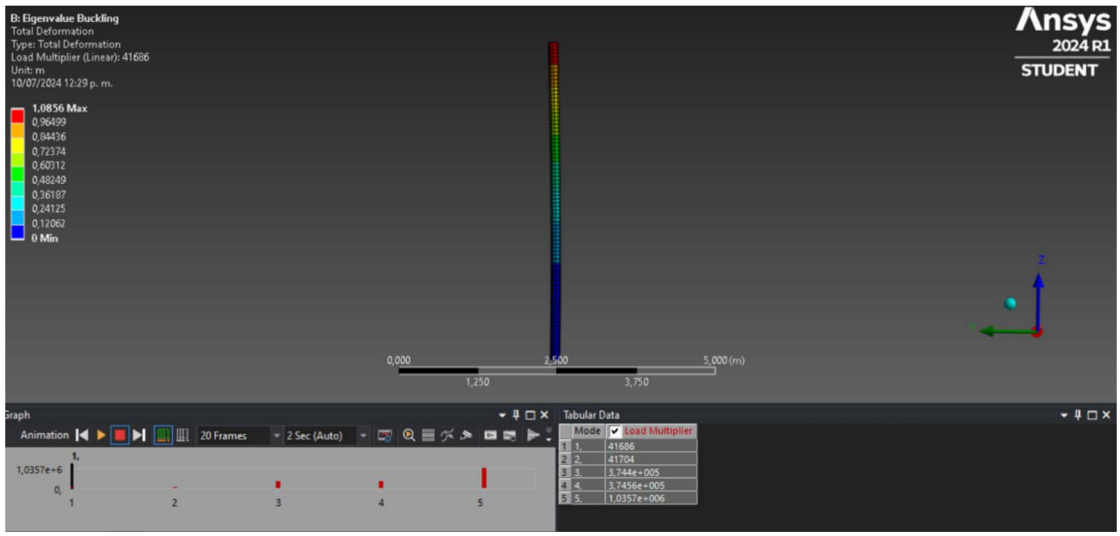

Figure 4: Concrete column simulated and its results.

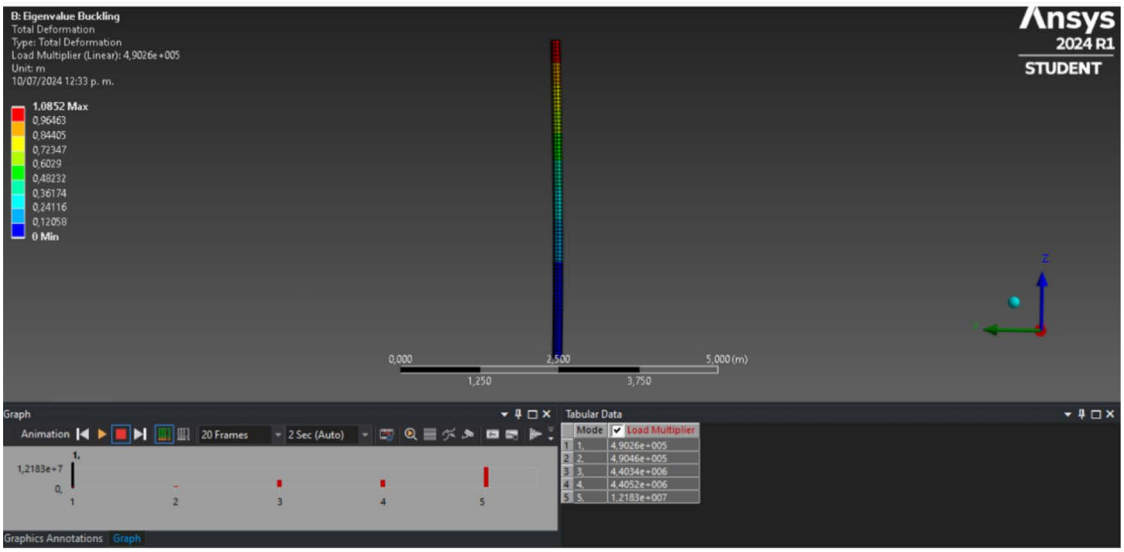

Figure 5: Structural steel column simulated and its results.

Using material selection criteria to highlight natural materials' potential for technical applications

University of Brescia, Italy

Supervisor: Stefano Pandini

Students: Vittoria Mandolini

Contents

1. Summary

In this study, we used Prof. Ashby's optimized material selection technique for mechanical design, combined with the Ansys Granta Edupack software, to identify the most effective natural materials for specific engineering categories such as stiff and light tie rods, strong and light beams, etc. We were able to rank, visually, and quantitatively, the performance of natural materials and highlight the most interesting using material performance indices, established by translating unique designs into functions, constraints, and objectives. The findings provided a platform for a more in-depth analysis of the best performing systems, aimed at understanding the reason for such a performance as based on composition and microstructure, as well as a comparison with synthetic materials.

2. Objectives

Biological evolution and engineering frequently have the same goal: to find optimal solutions that improve performance while using the least amount of energy possible. Component and microstructure optimization is the result of a long, selective evolution process, and it is frequently the root cause of extraordinary behaviour.

Traditionally, people have thought of natural and engineering materials as two distinct families, although, as "green" materials have gained popularity, this perspective has shifted. Indeed, when considering raw attributes and performance indicators for a certain application, the two families overlap significantly.

To better understand the potential of natural materials, the optimized material selection method of Prof. Ashby's [1] may be employed through the Ansys Granta Edupack's library of natural materials records. Highlighting which natural material has an excellent response may be useful for a variety of reasons. Primarily, when aiming to employ natural materials for a specific technical function, it

facilitates a straightforward comparison with conventional materials. Second, by identifying materials with outstanding performance, the technique will evidence interesting cases in which a detailed knowledge of the basis for such excellence, based on composition, chemistry, and microstructure, is warranted. Finally, recognizing the structure-property correlation underlying such performance could guide the development of new techniques through a biomimicking strategy.

3. Problem statement

Prof. Ashby's material selection approach provides a quantitative description of materials' performances for a specific application. Depending on the application, one can formulate the problem in various ways, typically by expressing its function, the primary and secondary constraints that the material must satisfy, an objective to rank material performances, and the free variables that serve as degrees of freedom for the optimal selection. For instance, when searching for a tie that is both stiff and light, we can formulate the problem arbitrarily as follows:

- Function: Tie under tension;

- Main constraint: stiffness, $S^* = F/A$ (F: axial force, A: cross-section);

- Additional constraint: natural material;

- Objective: minimize mass;

- Free variables: material choice, cross-section.

4. Proposed solution

The problem statement determines the material index, M, as well as the bubble chart for visual solutions (in the aforementioned case, $M = E/\rho$, where E is Young's modulus and ρ is density, and the plot to work with represents Young's modulus vs. density). We can find the specific index formula through a straightforward computation using the primary constraint and objective function, combining them through the free variables. However, for our examination of natural material performances, we may only refer to typical engineering and design scenarios, so the index may also be easily accessible through Granta (Booklet in the Learn section; Performance index finder in database Level 3).

The optimum solution can be expressed in terms of a ranking grid, by ordering the materials according to the material index, or graphically by using index lines in the bubble chart to quickly indicate which natural materials perform best.

The additional constraint regarding the material families may be applied by means of a "Tree" function, specifying the classes of natural materials of interest (in the following examples, we focused our attention on "natural materials," which are mainly wood and wood-like systems, soft tissues, mineralized tissues, natural fibers, and technical ceramics). Using a "Tree" function in the selection steps enables you to concentrate on specific materials when flagged, and to effortlessly compare them with all materials by deflagging.

5. Results and conclusions

The most well-known bubble chart, the Young's modulus vs. density plot, is used to demonstrate this research method. Figure 1 displays a plot of the approximately 4100 materials discovered in Granta (Edupack; Level 3), with over 500 belonging to five relevant classes of natural materials. This map depicts natural materials, grouped and partially overlapped, spanning about 2 decades of densities (100÷1000 kg m^{-3}) and 6 decades of stiffness (0.001÷1000 GPa). This picture clearly illustrates that natural materials cannot achieve the same stiffness or lightness of some synthetic materials, but reading about their performance in terms of material indices may help in highlighting their true capabilities for a certain function.

This entails defining a function (tie in tension, beam in bending, panel in bending, etc.) as well as the related performance index so to rank and compare the various materials performances. Table 1 ranks the top eight entries based on three functions, while Fig. 2 shows this graphically for the natural materials by reporting the index lines.

When it comes to stiff and light ties, apart from the case of spinel (a natural crystal commonly used in furnace bricks to improve refractoriness) fibers, woods, and mineralized tissues all rank highly. This raises issues regarding how and why such a performance is possible.

Fibers (Ramié, Hemp, Kenaf, with M_t = 0.03÷0.05 GPa m^3 kg^{-1}) are an interesting case: how can such flexible, mildly grown systems work so well? The response lies in striking the right balance between stiffness and lightness: highly orientated and aligned cellulose fibrils (M_t = 0.067 GPa m^3 kg^{-1} provide stiffness, outperforming glass fibers (M_t = 0.022 GPa m^3 kg^{-1}) and steel (M_t = 0.022 GPa m^3 kg^{-1}); on the other hand, the presence of voids reduces their density. Fibers that take advantage of cellulose rigidity perform the best: Ramié fibers are very effective due to their unique structure, which comprises of highly crystalline cellulose fibers combined with a high porosity, allowing them to absorb more than other fibers (Fig. 2a); hemp and flax, have a composite-like multicellular structure, with tangled cellulose-rich microfibers grouped in polygonal sections that run parallel to one another (Fig. 2b).

Wood (along the grain) ranks highly among solid materials. The structure is comparable to fibre-reinforced composites made of largely aligned cellulose fibers bonded by hemicellulose and lignin. The bubble of "natural materials" in Fig. 2, almost entirely composed of woods and wood-like materials, occupies a large area due to its vast stiffness and density. Their characteristics are based on both their anisotropic features (stiffness along and across the grain) and their microstructure (the shape and size of the prismatic cells, the vase diameter, and most importantly, their porosity). Here, the strong stiffness-density correlation is evident. Certain woods, however, outperform others in terms of characteristics (Kaneelheart is the stiffest and heaviest; Balsa is the least rigid and lightest) and performance indices (Table 1). Because of its unique polygonal tracheid structure, spruce provides the best combination of rigidity and lightness for a tie. Sitka, in particular, a kind of spruce found in Norway, has adapted to hard weather and high winds by growing hexagonal tracheid elements that appear like honeycombs and maximize material distribution (Fig. 2c).

One intriguing comparison is that woods perform similarly to femur and radius trabecular bones and epoxy resin/carbon fiber composite. Nature has a vast material potential compared to engineering materials, and structural optimization may allow nature to achieve performance levels equivalent to synthetic materials made from the best polymers and fibers.

When it comes to bending beams and panels, wood outperforms fibers and other materials, particularly those with a lower density. High porosity increases performance for indices such as M_b (for beams with free cross sections) and M_p (for panels with free thickness). Woods such as Balsa have a structure like that of spruce, but the larger cells and spongy fibers, which are abundant in lymphatic channels, increase the pore percentage to up to 90% (low density, LD, and Balsa have a relative density of 0.1) (Fig. 2d). PVC-based foams, ceramic foams, and SiC aerogels are examples of synthetic materials that aim to emulate this structure by combining a foam-like structure with a stiff matrix.

The method can be used for numerous functions and applications. A quick summary of strength and flexibility is offered. To investigate light materials' strength performance, Fig. 3 (top) shows a strength vs. density plot and index lines for tie, beams, and panels (M_t, M_b, and M_p, respectively). Fibers, particularly flax, kenaf, and banana, exhibit the best performances under tension due to the hydrogen bonding between cellulose and the remaining elements. Silkworm and spider fibers exhibit outstanding performances, as we will discuss below. While natural fibers don't perform as well as high-strength synthetic ones, we can compare them to rayon based on cellulose and Dacron based on polyester. In the beam bending criterion, fibers are again the best records, suggesting that the new bio-composites trend may find the best reinforcement in the most performing ones. Wood lower performances, both in tension and in flexure, are due to a statistical effect caused by solid materials having more flaws. Different types of wood perform best: on one side, compact woods like kauri, pine, and fir; on the other, wood-like materials like bamboo, which have strong walls around an empty inner core that enhance lightness. Interestingly, they perform similarly to epoxy-high-strength carbon fiber biaxially reinforced composites. Finally, spongy woods, such as balsa, are excellent for bending panels because of their high porosity. For the same reason, femoral bones, which are composed of much stiffer material, also perform well. Birds' spongy bones show this approach in action, but toucan's beak, with its cellular honeycomb structure that decreases density to 0.1 kg m^{-3}, or the void core hollow of the bird's feather (rachis), exhibits it at its best.

The ability of a material to deform significantly before failure is critical in many applications, including elastic hinges and shock absorbers. Researchers can measure this ability in terms of elongation at break or amount of energy absorbed before breaking. When such a behaviour is researched in compact structures (that is, with the objective of volume minimisation), the performance indices are $M_d = \sigma_t/E$ and $M_e = \sigma_t^2/E$, respectively (σ_t: tensile strength). A visual representation is shown in Fig. 3 (bottom), representing the Young's modulus vs. tensile strength bubble plot, with the two index lines operating towards minimisation (i.e., optimal solutions are the most distant below the line).

The representation is useful for ranking material performance, but in this case, some materials dominate the higher rank: spider silk, which has already shown to be particularly strong and light (Fig. 3 top), outperforms other fibers in terms of deformability and resilience; similarly, skin and cartilage excel among soft tissues.

Spider silk's exceptional behaviour depends on composition and structure. The fibers are mostly composed of fibroin (70–75%), bound and covered by sericin. Interwoven hard crystalline segments (crystalline sheet) provide strength to the fibers, while elastic semi-amorphous sections (spiral) with varying quantities of spiral structure contribute to their elasticity. Different glands can "draw" and diversify fibers into various types. The viscid fibers, which forms the web's spiral line and traps insects, is the most flexible and resilient component, with only β-spiral and no β-sheets. Due to the presence of β-sheets, the stiffer dragline (radial lines and web frame) provided ideal strength and lightness (Fig.

3 top). Due to their very different functions, the performance of these fibers is also superior to that of other natural silks, such as silkworm (Bombyx mori). Spider silk is designed to catch and trap flying insects and bear moving loads, whereas silkworm fiber have to shield the worm before breaking easily upon disclosure after worm metamorphosis.

When compared to other materials in terms of deformability, it performs similarly to polyurethane-based and butadiene rubber, as well as our natural elastic hinges, namely human skin and cartilage. In terms of energy absorption, it outperforms all manmade and natural materials, and its properties are comparable to Kevlar fibres.

In conclusion, in this work, we attempted to focus on the performance of natural materials using material selection approaches based on the concepts of function, requirements, and performance optimization. The strategy made it easier to identify the best natural materials for different design methods and compare them to engineering materials. A closer examination of the basis for this superiority revealed that natural materials are highly organised “objects”, where a precise design determined the direction and combination of various phases with different properties. The approach allowed for deep insights through a process comparable to “reverse engineering” applied to natural materials, revealing their entire performance potential, and possibly paving the way for future advancements in material science and sustainable design.

6. References

[1] M.F. Ashby, Elsevier Science & Technology (2016).

[2] K. Goda et al., Composites Part A: Appl Sci Manuf, 37, 2213 (2006).

[3] J. P. Manaia et al., Fibers, 7, 106 (2019).

[4] P. Karinkanta, Acta Univ. Oulu. C, 516 (2014).

[5] J. Brändström, IAWA Journal, 22, 333 (2001).

[6] J. Galos et al., Materials & Design, 221, 111013 (2022).

[7] M. Borrega et al., Wood Sci Tech, 49, 403 (2015).

7. Appendix

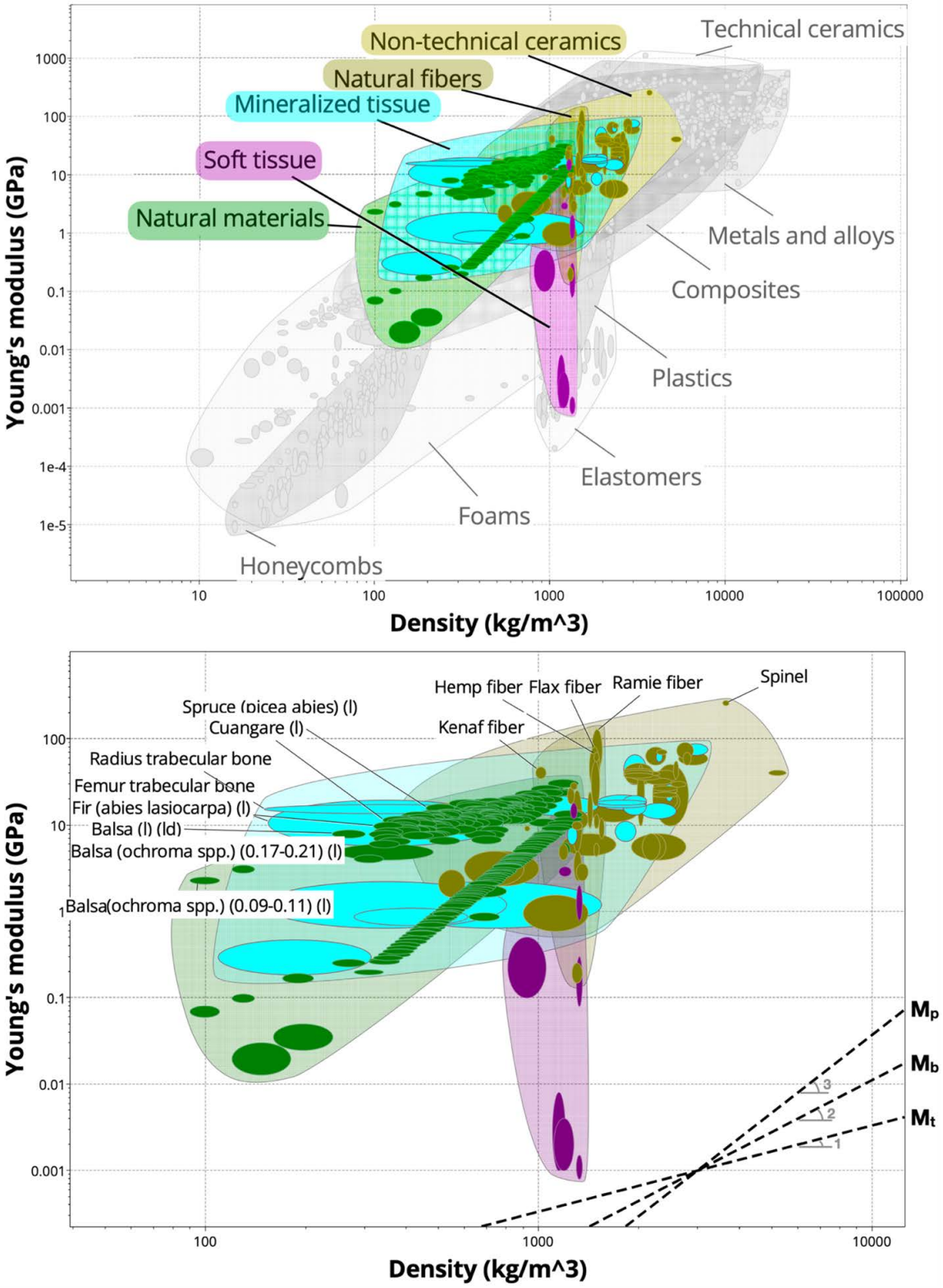

Figure 1: Young's modulus vs. density bubble chart. Top: all the materials are listed and the five class of natural materials selected are highlighted. Bottom: only he five class of natural materials selected are reported; labelled bubbles refer to the materials, listed in Table 1, that exhibit the best performances based on the different indices (M_t, M_b and M_p; the dashed lines are reported as graphical tools for the performance indices).

Table 1: Ranking of the best 8 natural materials based on the different functions (tie in tension; beam in bending; panel in bending) and the corresponding material performance indices (M_t, M_b and M_p, respectively; E: Young's modulus; ρ: density).

Function	Tie - tension $M_t = E/\rho$		Beam - bending $M_b = E^{1/2}/\rho$		Panel - bending $M_p = E^{1/3}/\rho$	
Rank	Material	Index, M_t (GPa m³ kg⁻¹)	Material	Index, M_b (GPa$^{1/2}$ m³ kg⁻¹)	Material	Index, M_p (GPa$^{1/3}$ m³ kg⁻¹)
1	Spinel	0.0713	Balsa (low density)	0.0152	Balsa (low density)	0.0132
2	Ramie fibres	0.0501	Balsa (mid density)	0.0136	Balsa (mid density)	0.0112
3	Radius trabecular bone	0.0445	Balsa (high density)	0.0114	Balsa (high density)	0.00855
4	Hemp fibres	0.0416	Radius trabecular bone	0.0113	Balsa	0.00744
5	Kenaf fibres	0.0400	Balsa	0.0105	Radius trabecular bone	0.00718
6	Flax fibres	0.0316	Femur trabecular bone	0.00941	Femur trabecular bone	0.00634
7	Spruce (along grain)	0.0311	Cuangare	0.00897	Fir (a. l.)	0.0605
8	Femur trabecular bone	0.0308	Fir (a. l.)	0.0884	Cuangare	0.0597

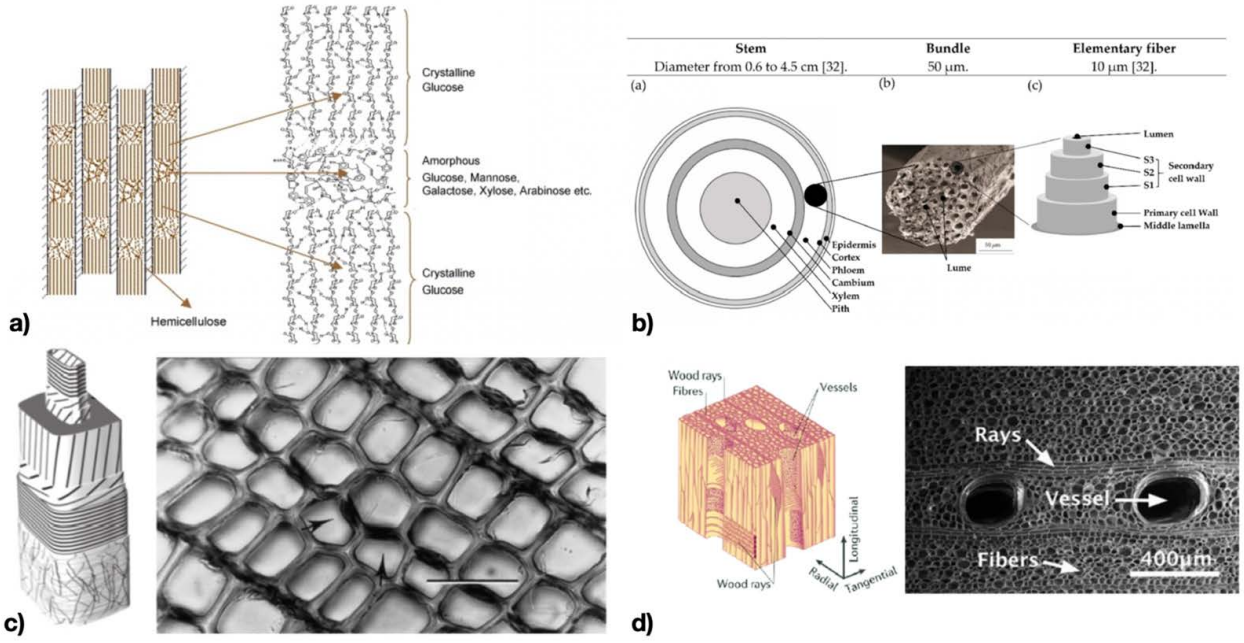

Figure 2: Representation of the different microstructure of a) ramie fibers [2], b) hemp fibers [3], c) Norway spruce [4,5], and d) Balsa [6,7].

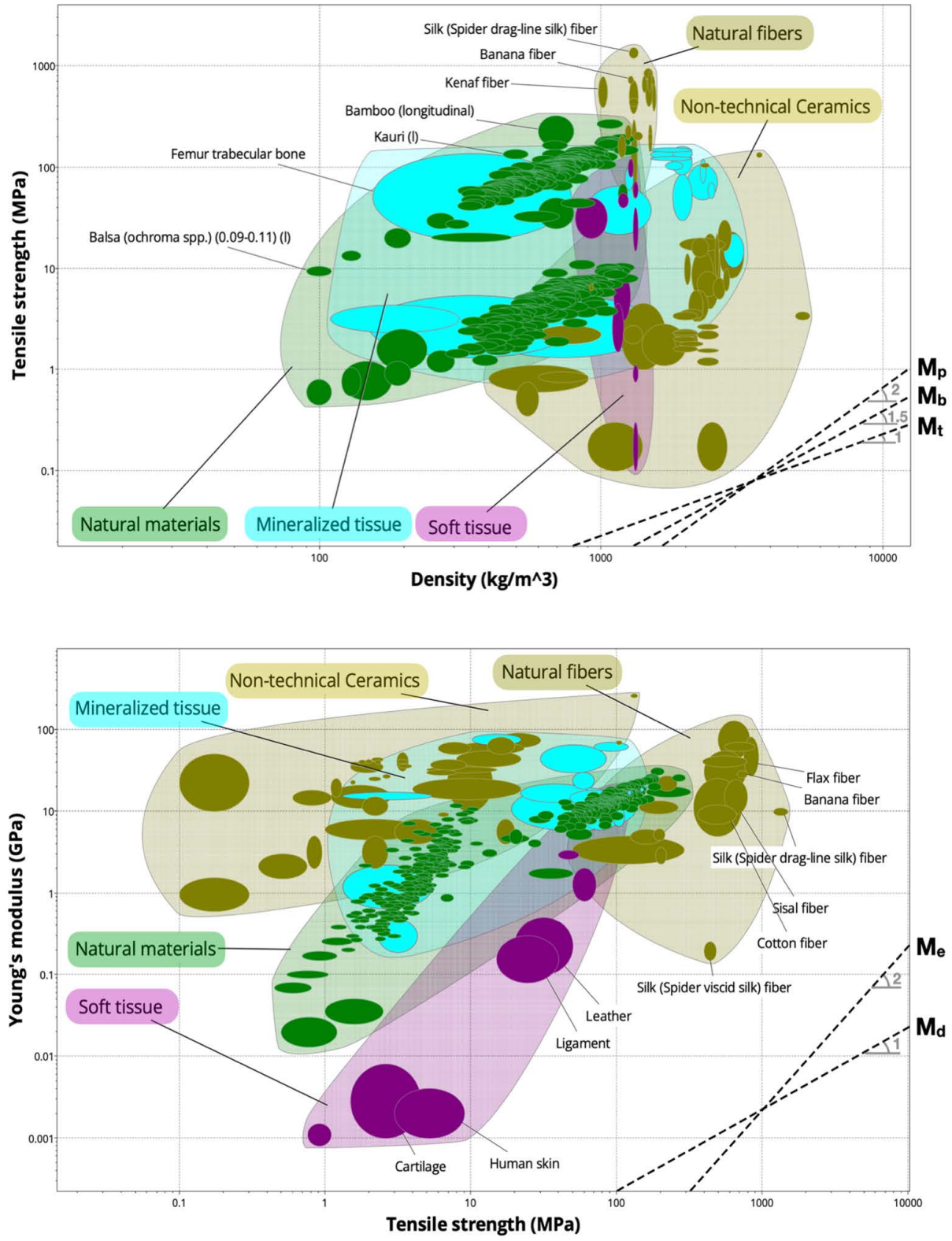

Figure 3: Top: Tensile strength vs. density bubble chart. Bottom: Tensile strength vs. Young's modulus bubble chart. Labelled bubbles refer to the materials that exhibit the best performances based on the different indices (dashed lines are reported as graphical tools for the performance indices).

Development of Climate Protection Technologies for Aircraft Speedometers

Universidade Estadual de Campinas, Brazil

Supervisor: Josué Labaki, PhD

Students: Esther Alves de Souza, Guilherme Fielder Frascati, and Hugo de Negreiros Moura

Contents

1. Summary

The Pitot tube is an essential device in vehicles such as aircrafts. Its application in measuring relative velocities is crucial for flight safety and for pilots' decision-making. In these cases, the Pitot tube must be capable of functioning under all conditions to which it is exposed. Though challenges like freezing can cause obstructions at its inlet. Therefore, this study utilizes the extensive range of Ansys software to propose a solution to the freezing problems of Pitot tubes, incorporating an internal heating system and an external coating of polytetrafluoroethylene (PTFE) due to its highly hydrophobic properties. Focusing on material selection using Ansys Granta EduPack, steel, aluminum, and PEEK/IM carbon fiber composites emerged as potential candidates for use in the Pitot tube, as they demonstrate excellent mechanical strength, low density, good thermal conductivity, and, except for the composite, relatively low associated costs. Furthermore, the selected materials were submitted to tests, first being the fluid dynamics simulation utilizing Ansys Fluent, in which the velocity and pressure fields were obtained. The latter was then utilized in the mechanical resistance simulation with Ansys Mechanical. After, two more simulations were done: thermal behavior utilizing Ansys Steady State Thermal and freezing patterns around the Pitot tube with Ansys FENSAP-ICE. The results pointed to a 95.9% reduction in the mass of ice accumulated in the Pitot tube with heating and the PFTE layer. For the material, aluminum was selected because it has the lowest cost and best thermal performance among the options evaluated.

2. Objectives

Using the features of Ansys Granta EduPack and other Ansys software, this work proposes to select appropriate materials for the construction of a Pitot tube capable of withstanding adverse conditions of thermal stress and icing. In this way, the innovations presented aim to overcome the common challenges faced by this instrument, which is susceptible to damage that interferes in its function as an aircraft speed measurement device.

3. Problem statement

The Pitot tube is an essential instrument for measuring relative velocity in various modes of transportation. It must be durable and designed with advanced technology to withstand the challenges of its operating environment, such as extreme temperatures and highly pressurized conditions. The accident involving Air France flight AF 447 [1] highlighted the importance of the sensor that, according to the final reports, was one of the main factors for the aircraft's crash. Other occurrences of accidents caused by Pitot tube icing [2] were the 1996 crash of Birgenair flight 301, involving a Boeing 757-225 on the route between the Dominican Republic and Frankfurt, Germany; the 1974 crash of Northwest flight 6231, involving a Boeing 727-251 on the route between New York City and Buffalo, USA; and the 1997 crash of Austral Líneas Aéreas flight 2553, involving a McDonnell Douglas DC-9-32 on the route between Posadas and Buenos Aires, Argentina. In total, 494 people died in the accidents mentioned, underscoring the importance of the present study. Thus, this project studies the functional structures of the Pitot Tube and propose a solution to its icing assisted by Ansys Granta EduPack.

4. Proposed solution

Pitot tube freezing demands design alternatives to avoid it, which yields in a variety of solutions and ways for improvement. Hence, a material selection was conducted utilizing Ansys Granta to mitigate Pitot tube freezing. One of the criteria was how materials interact with anti-freezing techniques that will be applied in the final product proposed in this work. The investigative route adopted consists of the definition of a flight case, and of the Pitot tube's necessities to bear it. After this, Ansys Granta was used for material selection, ensuring they are following the proposed case limitations. The materials will be subjected to simulations of their thermal behavior at the Ansys Steady State Thermal and their mechanical resistance with Ansys Mechanical. For the second analysis, the resultant pressure field will be imported from the fluid dynamics simulation of the proposed case at Ansys Fluent. At last, the Pitot tube freezing behavior will be analyzed through Ansys FENSAP-ICE. All analyses are extremely important to complement the material selection made on Ansys Granta to certify the proposed techniques' applicability and effectivity.

Among many situations that can lead to aircraft components freezing, a set of factors were selected based on the frequency that events were reported. The set consists of a commercial airplane, with horizontal velocity of 200 m/s [3,4], going through a frontal stratiform cloud, since they are commonly entered during flights, and impacts on high values of liquid water content (LWC), 0.2 g/m^3 on average [5]. Therefore, the flight height chosen is 6000 meters, knowing that it connotes a higher frequency of frontal stratiform clouds [5,6]. The air temperature selected was -10 °C, considering that most freezing reports are next to this temperature [6-8]. The freezing mechanism implemented is based on supercooled liquid droplets (SLD), in which those droplets, with average diameter of 35 micrometers [6,7,12], froze when accelerated by the airflow, potentially accumulating on the Pitot tube. Moreover, the freezing was considered to form rime ice instead of glaze ice, in the view that the former is significantly more reported in incidents than the latter [7].

To resist the freezing condition, an internal heater was added next to the tip of the Pitot, so that, defining the heating power, the orifice face temperature can be chosen. Also, hydrophobic materials were researched to coat the tube. Higher hydrophobicity values impact in higher contact angles and lower contact areas with the water droplets [9-11]. Discussing the ice interaction, the application of a hydrophobic coat increases the adhesion loss on the solid layer, accounted for the function "delamination and cracking" on Ansys FENSAP-ICE simulation.

Established the simulation conditions and anti-freezing techniques, it's possible to select the Pitot tube material on Ansys Granta. For that, performance indexes were defined based the requirements of an commercial flight. The material must be lightweight, cheap and must have good mechanical resistance. In addition, as there is an internal heating system, the selected material must have good thermal conductivity, in order to improve heat transfer from the heating system. Thus, it was defined as a first performance index M_1 (Appendix A Equation 1), being the density of the material divided by thermal conductivity and by the elastic resistance modulus. Furthermore, a second index M_2 (Appendix A Equation 2) was defined by substituting the yield stress by the price of the material. Then, multiple material classes were considered to find the best material that minimizes M_1 and M_2. Next, fluid simulation with Ansys Fluent proceeded accordingly to the proposed case. The pressure field generated by the simulation was utilized by Ansys Mechanical in order to analyze the mechanical strength of the materials in the Pitot tube. Thermal simulation with Ansys Steady State Thermal were conducted to find the heating power that yields in 0 °C at the aperture external face, being chosen as reference to analyze the thermal performance of the materials in relation to the energy expenditure needed for the heating. At last, to verify the applicability of the proposed solutions, freezing simulation with Ansys FENSAP-ICE were carried out with common pitot tubes in steel and with the proposed solution.

5. Results and conclusions

The Ansys Granta ample scope of materials was utilized to plot the selection graphs based upon the performance indexes M_1 and M_2. Since they need to be minimized, the desired material is close to the origin of the graphs. Through the results expressed on Appendix A, plastics and composites can be taken out of the selection, as they did not meet the thermal and mechanical resistance requirements. The first performance index placed steel and aluminum alloys as desirable for the Pitot's tube, while highlighting the composite PEEK/IM carbon fiber as an outliner in comparison to other similar yet discarded materials. The second performance index, now considering cost also focuses on aluminum and steel. Pure molybdenum was also highlighted given its proximity to the origin of the graph. Despite that, the industrial scale of the Pitot's tube production makes the utilization of the pure material inviable, as iron-molybdenum alloys are more commonly used but were not highlighted by the analysis. Therefore, low alloy steel 4340, aluminum alloy 6061 and PEEK/IM carbon were used in further simulations.

Meanwhile, the material selection for the external hydrophobic layer of the tube used, as a criterion, the contact angle of multiple polymeric external layers used in the industry. The materials were chosen based on their hydrophobic properties and ease of application over metals. The research points to PTFE as the most hydrophobic material, while also being commonly used in the industry, such in steel pans covering. Therefore, PTFE has well defined industrial processes for metal covering and thus being chosen as the material for the surface of the tube.

The software Ansys Fluent made possible to simulate the proposed flight case, allowing the creation of velocity and pressure fields along and around the tube. The results in Appendix B showcase the impact regions of the tube. The front and back regions presented higher pressures and, therefore, higher sheering by the fluid around them. This has direct implications on the mechanical and icing simulations. The first mentioned showed that the materials could easily handle the stresses, showcasing their structural viability. The results expressed in Appendix C show the equivalent Von Mises tensions, that have as a failure criteria the materials yield limit. The analyzed materials were far from reaching their

yield limit, indicating their good mechanical performance.

After that, the materials were exposed to the Ansys Steady State Thermal's thermal exchange. The software allows the observation of how the temperature profile behaves through the tip of the tube under the external influence of -10ºC and internal heating. The adopted simulation method was adding different values of power to the heater and identifying the final surface temperature as the result. In those tests, aluminum had the best performance given its higher heat transfer coefficient. The surface of the aluminum Pitot tube reached 0ºC with 15W of heating power, while steel required 20 W. The differences between the results in Appendix D are a margin for prioritizing aluminum in comparison to the other materials, while the composite has a thermal conductivity of two orders of magnitude below the others.

To try out the applicability of the proposed techniques, freezing simulations of the tube were conducted, one with the PTFE layer and heating element and another without. The cases expressed on Appendix E showcast the differences between the common Pitot tube, and the one with hydrophobic covering and internal heating. Without the proposed techniques the tube accumulated a mass of 6.83 g of ice, resulting in the closing of its opening and impacting on its ability to measure speed. On the other hand, the heating of the tip of the tube and reduction of the ice adhesion due to the hydrophobic layer led to an accumulation of 0.348 g of ice in the tube with the opening remaining unobstructed, allowing correct speed measurement during the flight. This result also indicates how the loss of the ice adhesion impacts on ice accumulation. The back part of the tube, since it deals with high sheering pressures, had smaller amounts of ice because the material could not stabilize in the region, which also happens on the tip of the tube.

The variety of Ansys's software used in this Project allowed a deep understanding of the mechanisms that surround the Pitot tube operation and its icing. A solution for icing could be developed, reducing 94.9% of accumulated ice on the Pitot tube. Within the low alloy steel 4037, aluminum alloy 6061 and PEEK/IM carbon fiber, the aluminum showed the best thermal performance for internal heating implementation. Therefore, to minimize casualties and make flights even safer, with the help of Ansys software, building a Pitot's tube in aluminum with an internal heater of 15 W and a surface cover of PTFE would make airplanes significantly better equipped to flight in freezing prone regions.

6. References

[1] Moraes. The importance of the Pitot Tube sensor in aircraft: A case study of Air France flight AF 447. Revista Conexão SIPAER. Open Journal Systems. Available from:http://104.236.28.163/index.php/sipaer/article/view/507/420
[2] Marques Lisboa, K. (2013). Aerothermodynamic analysis of an aircraft Pitot tube: conjugate model, hybrid simulation, and parametric design studies. Undergraduate Project, Federal University of Rio de Janeiro. Available from: https://pantheon.ufrj.br/bitstream/11422/9083/1/monopoli10005541.pdf
[3] How Much Faster is a Private Jet Than a Commercial Airplane? Going Beyond Airspeed - Blog - The Aviation Factory. The Aviation Factory. (n.d.). Avaliable from: https://www.the-aviation-factory.com/en/blog/how-much-faster-is-a-private-jet-than-a-commercial-airplane/
[4] How fast do planes fly?. AirAdvisor. (n.d.). Available from: https://airadvisor.com/en/blog/how-fast-do-planes-fly
[5] XIAOBO, Dong; XIAOSHEN, Sun; FEI, Yan; JIANNAN, Zhang; SHUYI, Wang; MIN, Peng; HAIPENG, Zhu. Aircraft Observation of a Two-Layer Cloud and the Analysis of Cold Cloud Seeding Effect. Frontiers In

Environmental Science. [S. L.], p. 1-10. mar. 2022.
[6] Jeck, R. K. (2008). Distance-Scaled Water Concentrations versus Mass-Median Drop Size, Temperature, and Altitude in Supercooled Clouds. Journal of the Atmospheric Sciences, 65(7), 2087-2106. https://doi.org/10.1175/2007JAS2522.1
[7] AC 00-6A - AVIATION WEATHER FOR PILOTS AND FLIGHT OPERATIONS PERSONNEL. [S. L.]: Federal Aviation Administration, 1975.
[8] Supercooled Water Droplets. Skybrary Aviation Safety. (n.d.). Available from: https://skybrary.aero/articles/supercooled-water-droplets
[9] Danish, M. (2022). Contact Angle Studies of Hydrophobic and Hydrophilic Surfaces. In: Thomas, S., Rezazadeh Nochehdehi, A. (eds) Handbook of Magnetic Hybrid Nanoalloys and their Nanocomposites. Springer, Cham. https://doi.org/10.1007/978-3-030-90948-2_24
[10] Staniscia F, Guzman HV, Kanduč M. Tuning Contact Angles of Aqueous Droplets on Hydrophilic and Hydrophobic Surfaces by Surfactants. J Phys Chem B. 2022 May 5;126(17):3374-3384. doi: 10.1021/acs.jpcb.2c01599. Epub 2022 Apr 25. PMID: 35468298; PMCID: PMC9082615.
[11] Law, Kock-Yee. "Water–surface interactions and definitions for hydrophilicity, hydrophobicity and superhydrophobicity" Pure and Applied Chemistry, vol. 87, no. 8, 2015, pp. 759-765. https://doi.org/10.1515/pac-2014-1206
[12] Supercooled Large Droplet Icing. NASA Glenn Research Center. (n.d.). Available from: https://aircrafticing.grc.nasa.gov/1_1_2_5.html

7. Appendix

a. Material Selection

$$M_1 = \frac{\rho}{\sigma_y^2 \lambda} \tag{1}$$

$$M_2 = \frac{\rho}{C_m \lambda} \tag{2}$$

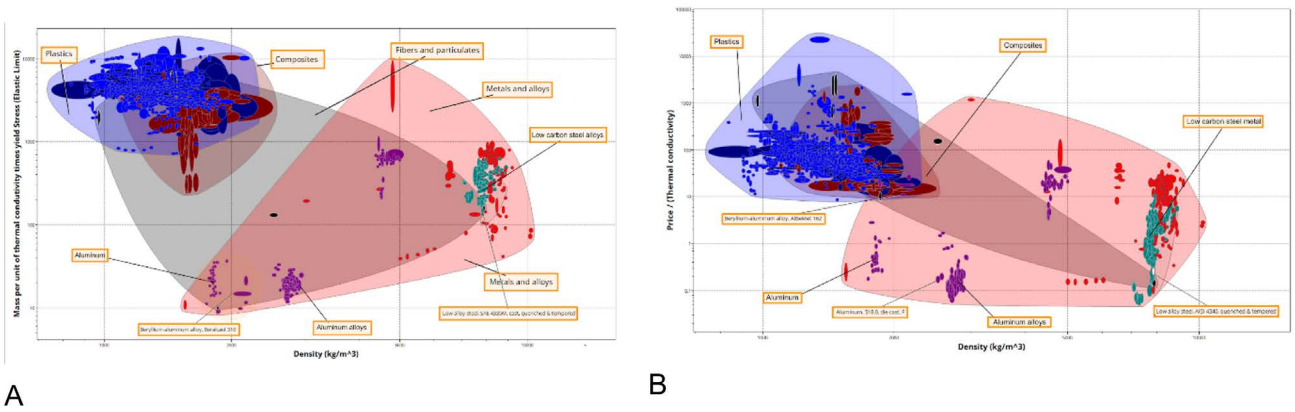

A B

Figure 1: Density scheme of materials that could be used to constitute the Pitot tube. The graph was made with the aim of minimizing the Merit Index from the Equation 1 (A). Scheme of price per thermal conductivity versus the density of materials that were critically compared to acquire the best solution according to the proposed objective. The graph was made with the aim of minimizing the Merit Index from the Equation 2 (B).

b. Ansys Fluent results

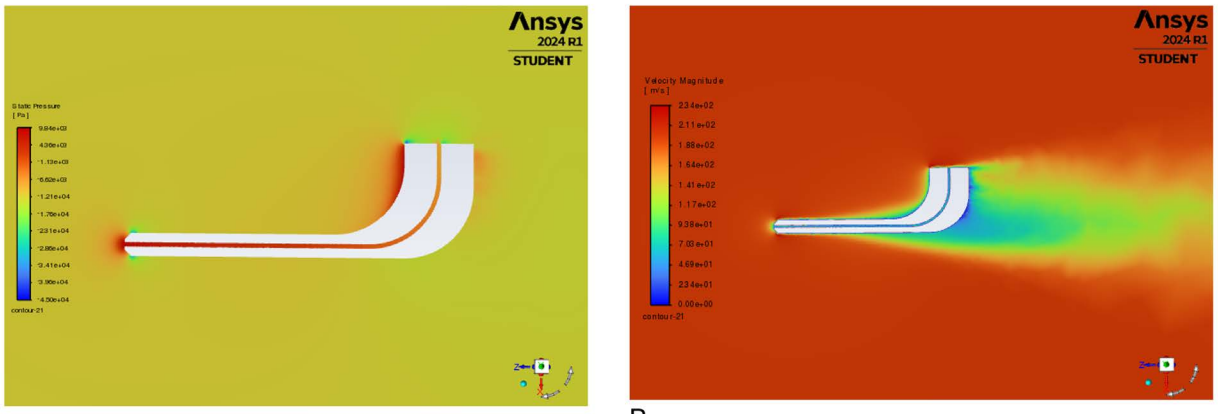

A B

Figure 1: Pressure field contours (A). Velocity field contours (B).

c. Ansys Mechanical results

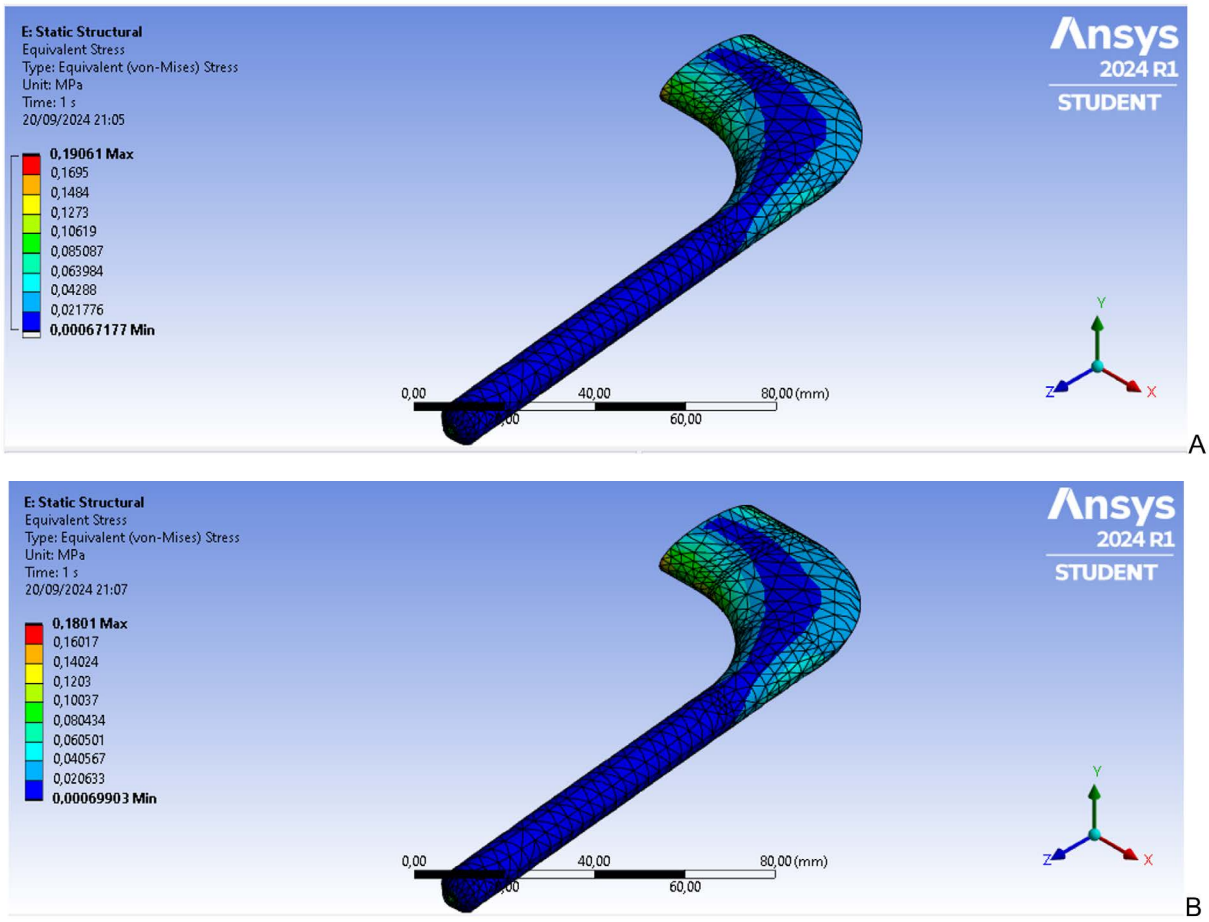

A

B

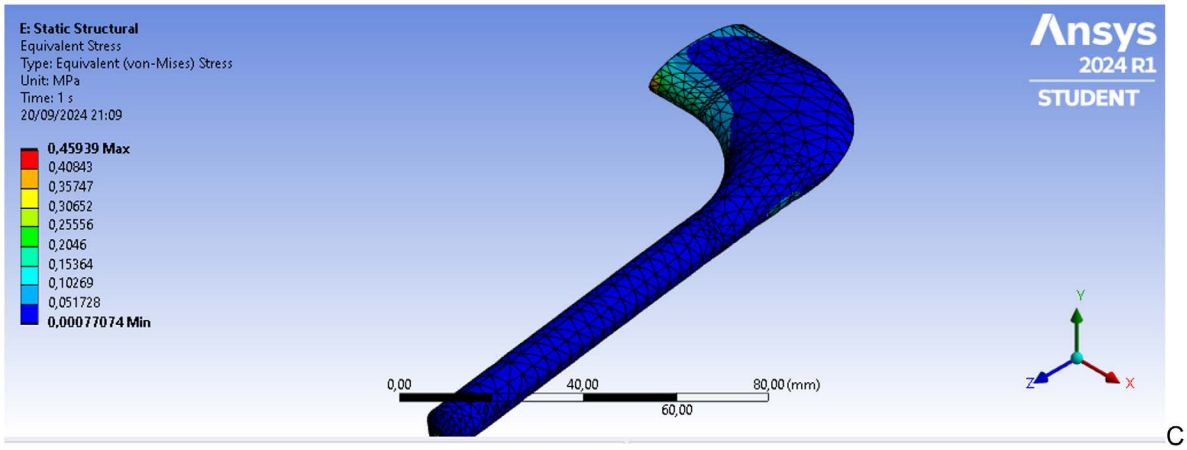

C

Figure 1: Equivalent Von-Mises stress for steel (A). Equivalent Von-Mises stress for aluminum (B). Equivalent Von-Mises stress for PEEK composite (C).

d. Ansys Steady State Thermal results

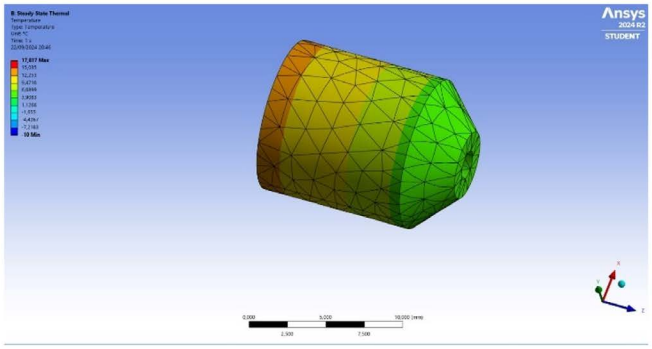

A

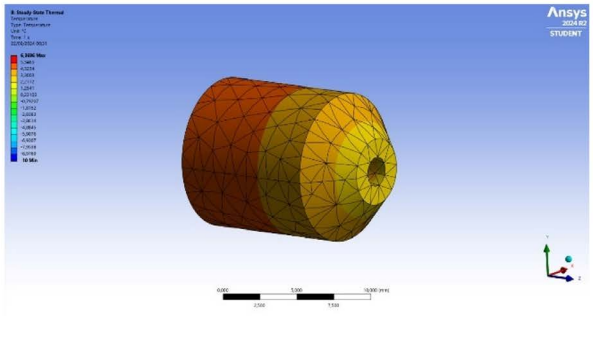

B

Figure 1: Temperature field for 20 W internal heating steel tube (A). Temperature field for 15 W internal heating aluminium tube (A).

e. Ansys FENSAP-ICE results

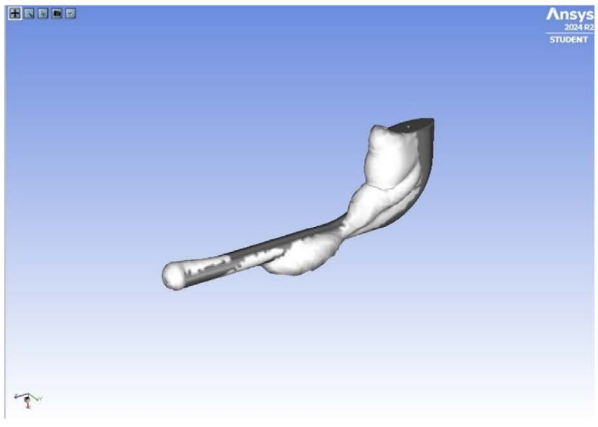

A

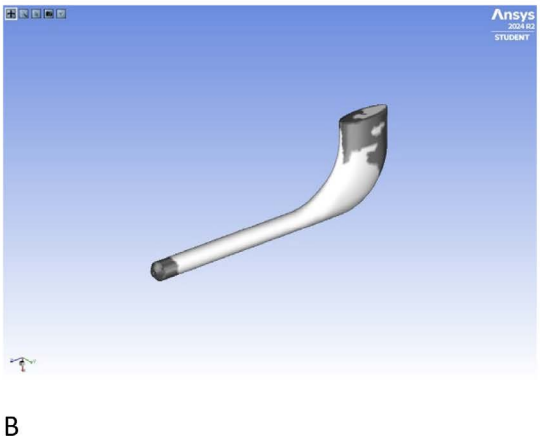

B

Figure 1: Ice accretion for the common Pitot tube (A). Ice accretion for the Pitot tube with PFTE layer and internal heating (B).

Eco-design for Smart Surfing Solutions with an Intelligent Iterative Design

University of Catania, Italy

Supervisor: Claudio Tosto

Students: Ivana Piccolo, Giovanni Sanfilippo, and Calogero Virzì

Contents

1. Summary

This work stems from the interest that emerged attending the class on Materials Science and Technology at the Engineering Faculty by two mechanical engineering students and a chemical engineering student with a passion for surfing. Surfboard fins are essential for stability, speed, and control in the water. With surfing's increasing prominence, especially following its inclusion in the Tokyo 2020 Olympic Games [1], there is a growing demand for high-performance fins. The surfboard market is projected to reach $2.6 billion USD by 2027 [2]. Fins are typically made from lightweight materials such as plastic, fiberglass, or carbon fiber, each offering varying degrees of stiffness and flexibility. Inexpensive fins, often made from polypropylene, are lightweight but provide limited performance. Fiberglass fins, while offering greater stiffness and a range of flex properties, add extra weight. There is a rising interest in sustainable surfboards and fins, with brands like Firewire and Channel Islands using recycled and bio-based materials to mitigate environmental impact [3]. Innovations such as 3D-printed surfboards made from recycled waste also present eco-friendly alternatives [4]. The ECOBOARD Project [5] demonstrates that these materials can reduce carbon footprints by 30%, highlighting a shift towards greener solutions in the surfing industry.

In this project, we aim to design a surfboard fin by substituting traditional materials (such as epoxy resin, fibers, and core materials) with alternatives that offer superior performance in terms of saltwater and UV resistance, low density, and high Young's modulus, while also incorporating a high renewable content. The key performance indicators (KPIs) for this study include these criteria. Using, and updating data when necessary, *Granta EduPack*, we select suitable material candidates by searching for a lightweight and economical internal core and an external skin made from a combination of resin and fibers, resulting in a durable and fully recyclable multi-layer structure with no impact on the environment.

2. Objectives

This project aims to design eco-friendly surfboard fins that minimize environmental impact while ensuring durability and performance. By integrating advanced technology—such as internal sensors placed at specific points through 3D printing of the core material—the fins enhance the surfing making possible the self monitoring and re-design of the fin.

The research focuses on optimizing both the internal core and the outer skin of a sandwich structure that constitutes the fin, although this approach can also be applied to the entire surfboard. The core is designed to be lightweight and cost-effective due to its higher volume ratio, while the skin's role is to provide mechanical performances and, at the same time, being a disassemblable structure allowing for material recovery and reuse. This design enables the recovery of most materials after use, without damaging the reinforcing fibers or any sensor elements.

The fin's skin is made from a hybrid laminate of carbon and natural fibers, aimed at reducing carbon content, and a recyclable matrix with high bio-carbon content. Additionally, non-aggressive recycling procedures are employed to ensure high thermo-mechanical properties are maintained throughout the lifecycle of the fin.

3. Problem statement

The design involves a sandwich structure that supports an adaptive fin system capable of being built, monitored, disassembled, redesigned, recycled, and remanufactured. This project considers composite manufacturing assisted by additive manufacturing (AM) techniques [6, 7], explored during the Lab Practice activities of the second semester of the 2023/24 academic year under the guidance of Prof. Claudio Tosto at the Polymers and Composites Lab (Department of Civil Engineering and Architecture, University of Catania), and supervised by Prof. Gianluca Cicala.

The materials for the core and skin of the fin are selected using the *Granta EduPack* software with the *Level 3 Sustainability* database. The skin materials must ensure resistance to saltwater and UV radiation while having a high percentage of renewable content. The software was initially used to determine the most suitable matrix material for the composite. In this project, we updated the existing database by incorporating data on additional materials identified by our research group [8-10] as suitable matrices. This database enhancement allowed us to get a more comprehensive material comparison without limiting the analysis to those already cataloged, demonstrating the potential of using *Granta EduPack* for customized, sustainable material selection for novel composites development.

The sandwich structure must enable a recyclable multi-layer system with minimal carbon content without compromising performance to satisfy green design requirements. The multi-layer structure was conceived featuring a hybrid composition of carbon and natural fibers to enhance sustainability without compromising performance, with natural fibers placed internally rather than on the outer layer to prevent moisture absorption and degradation from environmental and saline conditions. The *Synthesizer Tool* was used to design the composite and subsequently the multi-layer material. Regarding the core material, it is crucial to evaluate thermomechanical and physical properties, including durability, lightweight characteristics with good impact resistance, and an appropriate glass transition temperature. These factors are important not only for operational performance but also for composite manufacturing and potential post-curing processes intended to enhance the composite's thermomechanical properties. To identify a suitable printable and lightweight core material, the selection was narrowed down to polycarbonate (PC) and polyamide 11 (PA11) using the *Comparison Table Tool*.

4. Proposed solution

The primary research focused on selecting the matrix for composite materials. Initially, all material families were considered using a *Chart* that provided a general overview of the Young's modulus-to-density ratio (Figure 1). The *Tree Tool* was then used to narrow down the selection to thermosets (Figure 2). The *Limit Tool* was applied to exclude materials with unacceptable saltwater and UV radiation resistance (Figure 3), which removed a significant number of resins from consideration. Another *Limit* was set to refine the search to materials with more than 20% renewable content (Figure 4). The *Performance Index* was used to determine which resin would minimize mass and cost (Equations 1 and 2, Figure 5). Since the remaining resins had comparable values, the *final selection* was based on the maximum level of renewable content (Figure 6). After choosing the resin, a material combination was explored using the *Synthesizer Tool*. Initially, the *Composites – Continuous Fiber model* was employed to create composite materials with carbon fibers (Figure 7) and flax fibers (Figure 8). Next, using the *Multi-layer Materials model* (Figure 9), a 3-layer structure was selected, based on the previously created composites. The final step involved creating the sandwich structure (Figure 10) using the *multi-layer laminate* as the face-sheet and comparing different core materials.

5. Results and conclusions

Using *Ansys Granta EduPack* and following the Ashby materials selection methodology [11], we selected appropriate material candidates for the surfboard fin. The initial results focused on choosing the resin for the composite materials. Given its position as the outer coating of the fin, it was crucial to apply constraints for resistance to saltwater and UV radiation. With the added requirement for a significant level of renewable content, only 10 out of 57 initial thermosets met the criteria. Based on its excellent performance regarding the KPIs, we selected the 305 Epoxy Resin by ENTROPY RESINS [12]. This resin systems were added to *Granta EduPack* database to enrich the material selection options while anchoring it to data already present in the original database. This approach was chosen to demonstrate how *Granta EduPack* can be routinely updated with newer market developments allowing to have a flexible design tool.

The final skin consists of a multi-layer material organized as follows:

- Layer 3 (top): 0.15 mm of composite made with Super Sap 305 Epoxy Resin (CPS) and Carbon Fibers.
- Layer 2 (middle): 0.7 mm of composite made with Super Sap 305 Epoxy Resin (CPS) and Flax Fibers.
- Layer 1 (bottom): 0.15 mm of composite made with Super Sap 305 Epoxy Resin (CPS) and Carbon Fiber.

For the core material, we initially compared PC and PA11 (Figure 11), both suitable for AM. The comparison indicated that PC was favorable in most respects, although its renewable content was lower. However, this factor was less critical since the goal was to create a disassemblable external structure that, through the resin system, would enable the recovery of most fibers, the entire core, and any internal sensors [10]. PC was ultimately chosen as the core material due to its cost and Young's modulus, even in the comparison table for sandwich structures created by the *Synthesizer Tool* (Figure 12). The final properties of the proposed structure are shown in Figure 13. To expand this case study, integrating the system into software like *Ansys Fluent* for further testing of material properties would be advantageous. Preliminary work has been conducted using *Discovery* and *Ansys Fluent,* where we analyzed trends in velocity, static pressure on the fins, and the forces of lift and drag on a surfboard with a thruster setup featuring three fins (Figures 14-16). Based on these simulations, it can be

concluded that the chosen combination of materials is suitable for surfboard fin manufacturing as demonstrated by our laboratory trials (Figure 17). The final step will involve field testing the fins in real wave conditions, conducted by Ivana, our surf lover teammate (Figure 18). This will allow us to move the research from the lab to real-world scenarios.

6. References

[1] https://isasurf.org/event/tokyo-2020
[2] https://doi.org/10.3390/app12073297
[3] https://surfd.com/2023/05/riding-the-green-wave-sustainability-in-surfing/
[4]https://www.imperial.ac.uk/news/181048/imperial-researcher-develops-recyclable-surfboard-world/
[5] https://ecoboard.sustainablesurf.org/lifecycle-analysis/
[6] https://doi.org/10.1002/masy.201900069
[7] https://doi.org/10.1002/masy.202000256
[8] https://doi.org/10.1002/pc.24582
[9] https://doi.org/10.1016/j.jclepro.2021.127158
[10] https://doi.org/10.1002/masy.202200189
[11] Ashby, M. F. (2016). Materials selection in mechanical design(5th ed.). Butterworth-Heinemann.
[12] https://entropyresins.com/app/uploads/sites/2/2020/01/305-TDS-20200615-New-2.pdf

7. Appendix

Set of equation used as Performance Index:

$$M_1 = \frac{C_m \rho}{E_f^{\frac{1}{3}}} \qquad \text{(eq. 1)}$$

$$M_2 = \frac{\rho}{E_f^{\frac{1}{3}}} \qquad \text{(eq. 2)}$$

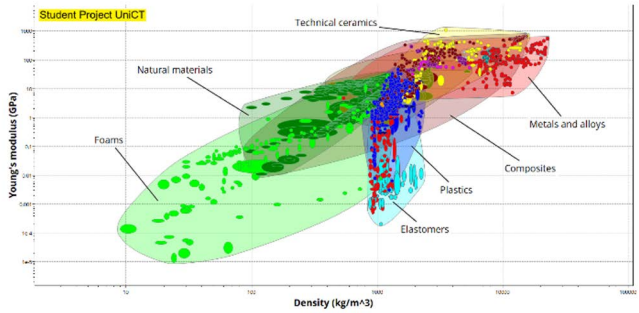

Figure 1: Chart with density in X axis and Young's Modulus in Y axis.

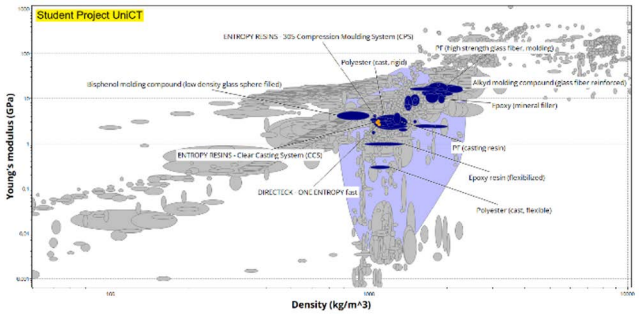

Figure 2: Using of Tree stage in order to select the thermoset materials.

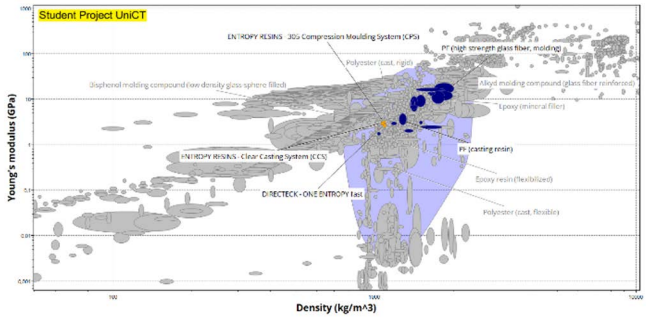

Figure 3: Using Limit tool in order to insert the UV radiation and saltwater resistance (acceptable).

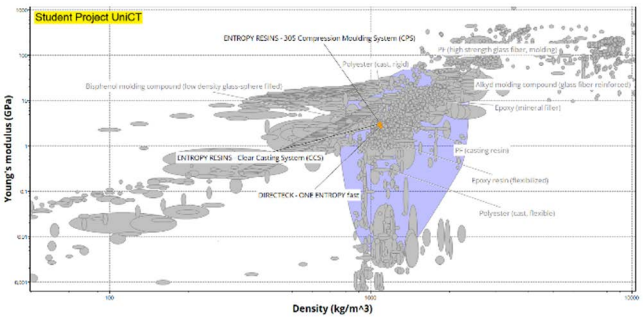

Figure 4: Using Limit tool in order to insert the renewable content (minimum 20%).

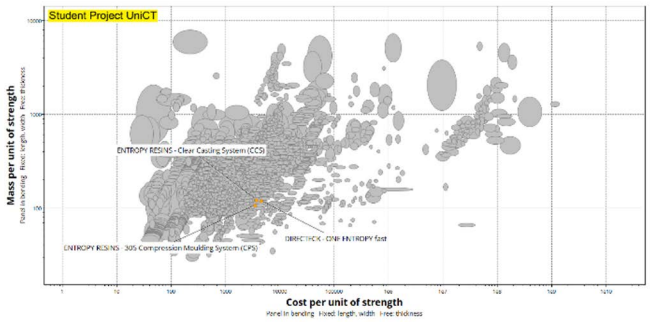

Figure 5: Using Performance Index. Panel in bending, minimize mass and cost.

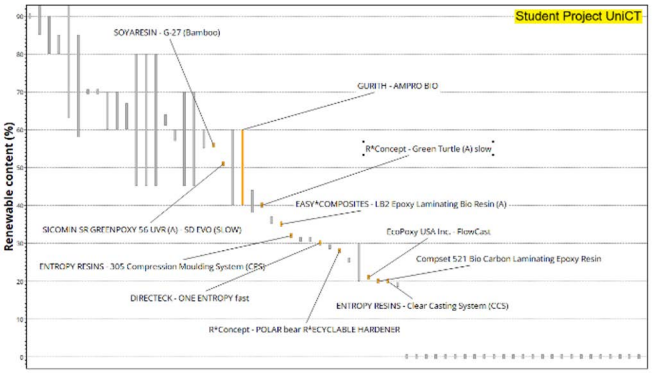

Figure 6: Realize a chart with renewable content in Y axis.

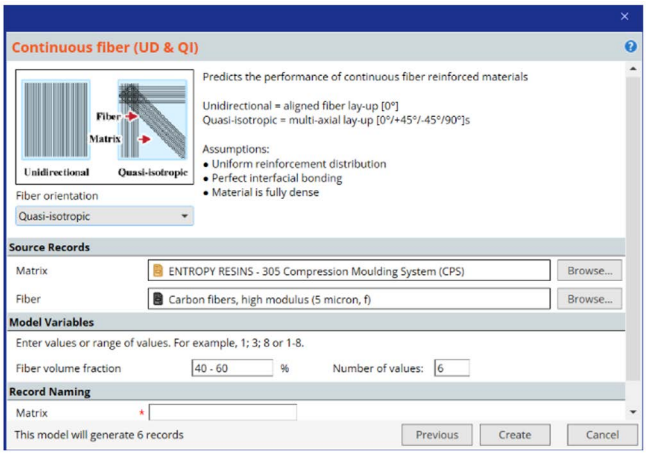

Figure 7: Using the Synthesizer toll in order to realize the composite material made of carbon fiber.

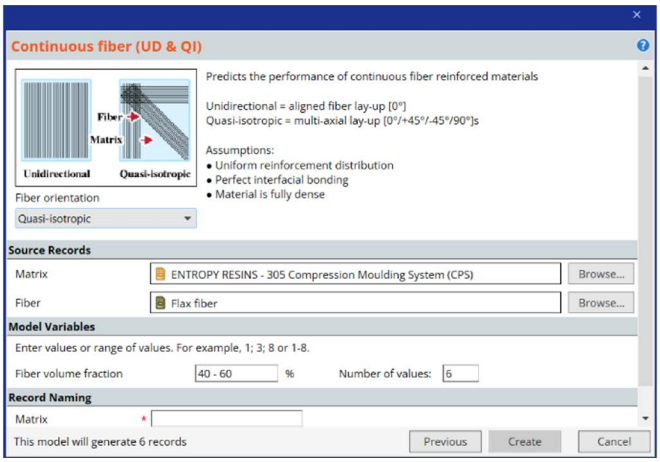

Figure 6: Realize a chart with renewable content in Y axis.

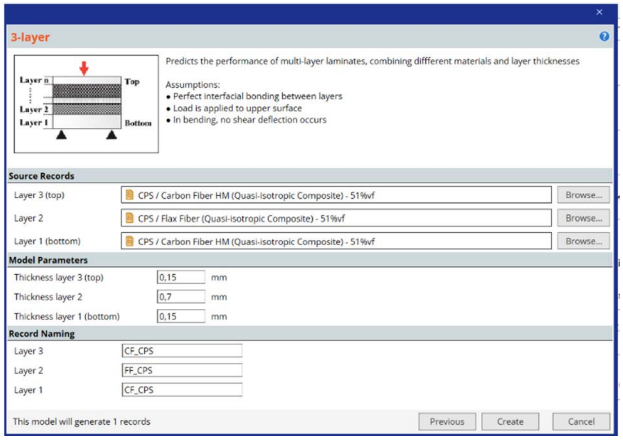

Figure 9: Using the Synthesizer tool to realize the multi layer structure with selected materials.

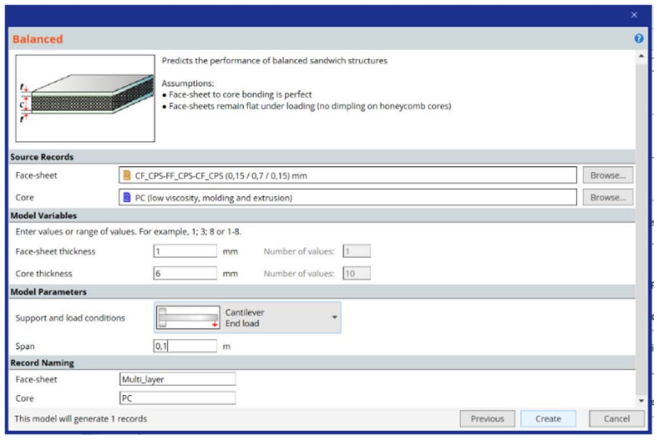

Figure 10: Example of a sandwich structure realized with the Synthesizer tool.

	PA11 (rigid)	PC (high viscosity, molding and extrusion)
Composition overview		
Renewable content (%)	100	0 ⇩
Price		
Price (EUR/kg)	21 - 21,6	3,12 - 3,39 ⇩
Physical properties		
Density (kg/m^3)	1020 - 1040	1190 - 1210 ⇧
Mechanical properties		
Young's modulus (GPa)	1,06 - 1,33	2,32 - 2,44 ⇧
Tensile strength (MPa)	50 - 55	62,7 - 72,4 ⇧
Flexural modulus (GPa)	1,09 - 1,3	2,27 - 2,34 ⇧
Flexural strength (modulus of rupture) (MPa)	56,9 - 69,6	86,2 - 93,1 ⇧
Durability		
Water (salt)	Excellent	Excellent
UV radiation (sunlight)	Fair	Fair

Figure 11: Comparison table between PA11 and PC.

	1mm Multi_layer face-sheets / 6mm PC core (Cantilever, End load, 0,1m span)	1mm Multy Layer face-sheets / 6mm PA11 core (Cantilever, End load, 0,1m span)
Price		
Price (EUR/kg)	9,84 - 10,1	23 - 23,7 ⇧
Physical properties		
Density (kg/m^3)	1230 - 1240	1100 - 1110 ⇩
Mechanical properties		
Young's modulus (GPa)	11,5 - 11,6	10,6 - 10,8 ⇩

Figure 12: Comparison table between sandwich structure with core made by PC or PA11.

Ansys 1mm Multi_layer face-sheets / 6mm PC core (Cantilever, End load, 0,1m span)

GRANTA EDUPACK

Price				
Price	9,84	-	10,1	EUR/kg
Physical properties				
Density	1,23e3	-	1,24e3	kg/m^3
Mechanical properties				
Young's modulus	11,5	-	11,6	GPa
Yield strength (elastic limit)	285	-	319	MPa
Notes				
Expected failure mode = core failure				
Flexural modulus	22,8	-	22,9	GPa
Notes				
Contribution due to core shear = 3,22%				

Figure 13: Properties of the sandwich structure.

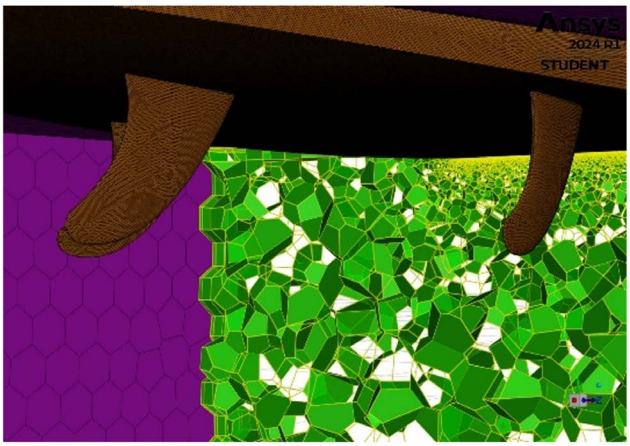

Figure 14: Mesh used in Ansys Fluent in the boundary zone of a surfboard with a thruster setup.

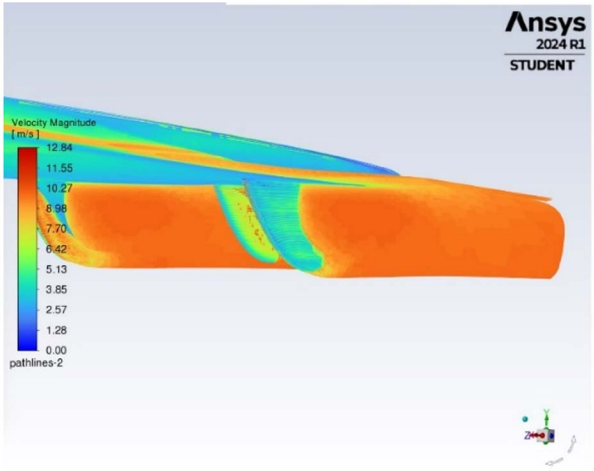

Figure 15: Trend of velocity magnitude in Ansys Discovery.

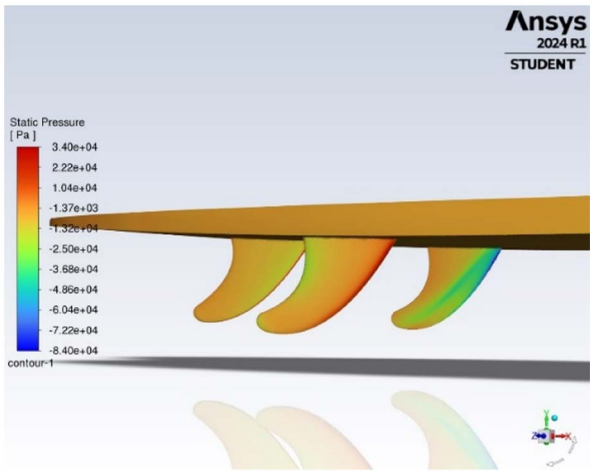

Figure 16: Trend of static pressure in Ansys Discovery.

(a) (b) (c)

Figure 17: Stages of the fin manufacturing process: (a) 3D printing of the core material; (b) some components for vacuum-assisted resin infusion; (c) Preparation of fabrics and resin.

Figure 18: Manufactured surf fin.

Hydrogen Embrittlement and Permeation in Materials for Hydrogen Transport: Challenges and Solutions

Universidad Pontificia Bolivariana,
Medellín, Colombia

Supervisor: H. Vladimir Martínez-Tejada
Students: Leonardo Pérez De los ríos, Sofía Vanegas Díaz, and Samuel Moreno Madrid

Contents

1. Summary

The research investigates the challenges and solutions related to hydrogen embrittlement and permeation in materials used for hydrogen transport. It explores the impact of hydrogen on the mechanical properties of pipeline materials and conducts a material selection process using Ansys Granta EduPack software, focusing on polymeric materials for their potential in transporting pure hydrogen and hydrogen-natural gas blends. The study identifies high-density polyethylene (HDPE) and polyimide (PI) as promising candidates for hydrogen transportation applications due to their resistance to hydrogen embrittlement. The findings contribute to developing safer, more reliable, and cost-effective hydrogen infrastructure, particularly in regions with existing natural gas pipelines, supporting the global transition towards a hydrogen-based economy.

2. Objectives

- To investigate the impact of hydrogen on the fracture toughness and yield strength of pipeline materials.
- To identify suitable polymeric materials that exhibit resistance to hydrogen embrittlement for hydrogen transportation applications.
- To contribute to developing safer, more reliable, and cost-effective hydrogen infrastructure, particularly in regions where natural gas pipelines are already in place, thus supporting the global effort to transition towards a hydrogen-based economy.

3. Problem statement

Hydrogen is expected to reduce CO_2 emissions by approximately 560 Mt annually in the European Union by the year 2050, significantly contributing to carbon neutrality goals (Fuel Cells and Hydrogen

2 Joint Undertaking, 2019). The implementation of hydrogen-based technologies is already underway in several countries. For instance, in Colombia, ambitious targets have been set for using green and blue hydrogen, with the aim of positioning the country as a regional leader in this technology by 2030 (Ministerio de Minas y Energía de Colombia, 2020). However, the transition to a hydrogen-based economy presents challenges related to hydrogen embrittlement (HE), which can compromise the structural integrity of pipelines (Kanesugi et al., 2023). The key issue lies in identifying materials that can safely and efficiently transport hydrogen without succumbing to HE, especially when adapting existing natural gas infrastructure for hydrogen transport.

Polymers and polyimides have demonstrated good resistance to hydrogen, particularly in low-pressure applications. Studies indicate that pipes made from these types of polymers can transport hydrogen at 100% capacity under low pressures without compromising material integrity. Nevertheless, it is essential to address the high permeability of hydrogen compared to natural gas, which can lead to losses and significant challenges that must be overcome before full-scale implementation (American Gas Association, 2023). This research aims to evaluate the impact of hydrogen on mechanical properties and conduct a material selection process to identify suitable polymeric materials for hydrogen transportation.

4. Proposed solution

The analytical methodology employed in this research involved a combination of a mathematical model and the selection of candidate materials using Ansys Granta EduPack. Firstly, while a pipe can be approximated as a cylindrical vessel subjected to internal pressure, for demonstrative purposes, a thin-walled spherical vessel subjected to the same conditions was considered. This choice was made because its wall stress and the most critical wall stress of a cylindrical vessel under those conditions are equivalent. Additionally, the properties represented by the indices depend on the material itself rather than the geometry.

For the development of the mathematical model, safety and lightweight requirements were considered. Based on these, failure criteria were developed to ensure that the vessel would not fail due to yielding or sudden fracture (equations 1 and 2). Considering these criteria and the critical wall stresses of the vessel, two performance equations were derived (equations 3 and 4), from which two property indices were sought to be minimized (equations 5 and 6), aiming for the lightest possible vessel. These equations are related through a coupling coefficient (***Cc***), which allows the search for suitable materials within Ansys Granta EduPack. The relationship between these performance equations is described by equation 7.

To obtain the slope of the optimization lines in the M1 vs. M2 graph, it was assumed that the crack size (***a***) is equal to the vessel's wall thickness (***t***). This assumption represents the most critical case when sudden failure occurs due to hydrogen embrittlement, as shown in Figure 1. Thus, to obtain values of the coupling coefficient, two crack sizes were considered: a relatively small one (5 µm) and a larger one (5 mm), covering a wide range of possible cases and allowing material selection based on specific requirements.

5. Results and conlusions

Based on the topographic maps obtained with Ansys Granta EduPack (Figure 2), the predominance of polymeric materials, specifically HDPE and PI, can be observed. These materials possess ideal physical

and mechanical properties that ensure their suitability for applications exposed to phenomena such as hydrogen embrittlement. In fact, numerous studies support this decision. The Plastic Pipe Institute (PPI) concluded that it is safe and feasible to transport hydrogen at a 100% concentration at pressures up to 2 bar and temperatures up to 140°F using pipes made of these materials, demonstrating adequate resistance to degradation. These findings are expected to contribute to the development of safer, more reliable, and cost-effective hydrogen infrastructure, particularly in regions where natural gas pipelines are already in place. By addressing the challenges associated with hydrogen embrittlement and identifying suitable polymeric materials, this research supports the global effort to transition towards a hydrogen-based economy (American Gas Association, 2023).

It has been proven that, both in the short and long term, using these networks for transporting pure hydrogen or mixtures of hydrogen with natural gas does not present degradation problems over exposure times ranging from 1 to 10 years. Previous experiences with the use of these networks provide a solid foundation for decision-making, as cities worldwide, such as Hawaii, Hong Kong, and Singapore, have used these types of pipes for transporting hydrogen-natural gas mixtures for many years (American Gas Association, 2023).

The selection of materials from different families to polymers (metals) is inappropriate given they do not fully meet the proposed requirements for the design of the specific component, with one of those being low density, which would substantially reduce the weight of the component. Additionally, the embrittlement and issues arising from hydrogen exposure to such materials must be considered. Studies have demonstrated that in duplex steels (ferritic and austenitic phases), hydrogen accumulates at grain boundaries, exacerbating structural embrittlement at microscopic scales. Similarly, in a titanium alloy (Ti-6Al-4V with compact hexagonal alpha and body-centered cubic beta phases), the formation of titanium hydrides and surface cracks was observed, particularly in the alpha phase and phase boundaries (Kim & Tasan, 2019). The magnitude of this problem has led to certain regulations, such as the ASME B31.12 Code for hydrogen pipelines, recommending against the use of materials like cast iron or high-nickel steels. These materials are particularly susceptible to hydrogen embrittlement (Raju et al., 2022). Other materials commonly used in pipelines, such as cast iron, pose a high risk of hydrogen leaks. Being heterogeneous alloys (containing multiple constituents in distinct phases within their microstructure), they inherently exhibit brittleness and porosity due to impurities, which may compromise their ability to withstand high pressures (Byrne et al., 2023; Speight, 2014).

The polymers highlighted in this article have not only been used for H_2 transportation but also for its storing. Studies on hydrogen storage tanks with PI and HDPE linings reveal that operating conditions affect the material's diffusivity and yield strength: an increase in temperature enhances hydrogen diffusion but reduces yield strength. Under certain conditions, this can lead to blistering, fractures, and material whitening due to gas nucleation in the pores (Yersak et al., 2017). Furthermore, pipes in regions with high temperature and soil acidity show greater degradation, underscoring the importance of the environment on the durability of these materials (De Silva et al., 2018). Although analyzing the effect of the environment and operating conditions on the failure time and integrity of pipeline networks and storage tanks made of these materials is beyond the scope of this research, it is a crucial aspect that must be considered in future projects related to this topic.

6. References

American Gas Association. (2023). *Impacts of Hydrogen Blending on Gas Piping Materials.*
Ashby, M. F. (2011). *Materials Selection in Mechanical Design* (4th ed.). ELSEVIER Ltd.
Budynas, R. G., & Sadegh, A. M. (2020). *Roark's Formulas for Stress and Strain* (9th ed.). Mc GrawHill.
Byrne, N., Ghanei, S., Espinosa, S. M., & Neave, M. (2023). Influence of Hydrogen on Vintage Polyethylene Pipes: Slow Crack Growth Performance and Material Properties. *International Journal of Energy Research*, 2023. https://doi.org/10.1155/2023/6056999
De Silva, R., Hilditch, T., & Byrne, N. (2018). Assessing the integrity of in-service polyethylene pipes. *Polymer Testing*, 67, 228–233. https://doi.org/10.1016/j.polymertesting.2018.03.001
Fuel Cells and Hydrogen 2 Joint Undertaking. (2019). *Hydrogen Roadmap Europe: A SUSTAINABLE PATHWAY FOR THE EUROPEAN ENERGY TRANSITION HYDROGEN ROADMAP EUROPE.* https://doi.org/10.2843/249013
Kanesugi, H., Ohyama, K., Fujiwara, H., & Nishimura, S. (2023). High-pressure hydrogen permeability model for crystalline polymers. *International Journal of Hydrogen Energy*, 48(2), 723–739. https://doi.org/10.1016/j.ijhydene.2022.09.205
Kim, J., & Tasan, C. C. (2019). Microstructural and micro-mechanical characterization during hydrogen charging: An in-situ scanning electron microscopy study. *International Journal of Hydrogen Energy*, 44(12), 6333–6343. https://doi.org/10.1016/j.ijhydene.2018.10.128
Ministerio de Minas y Energía de Colombia. (2020). *Hoja de ruta del hidrógeno en Colombia.* https://minenergia.gov.co/documents/10192/24298/Hoja_Ruta_Hidrogeno_Colombia.pdf
Raju, A., Martinez, A., Lever, O., Penchev, M., Lim, T., Todd, M., Lever, E., & Mathaudhu, S. (2022). *Hydrogen Blending Impacts Study.*
Yersak, T. A., Baker, D. R., Yanagisawa, Y., Slavik, S., Immel, R., Mack-Gardner, A., Herrmann, M., & Cai, M. (2017). Predictive model for depressurization-induced blistering of type IV tank liners for hydrogen storage. *International Journal of Hydrogen Energy*, 42(48), 28910–28917. https://doi.org/10.1016/j.ijhydene.2017.10.024

7. Appendix

Relevant equations

$$\sigma_{wall} \ll \sigma_y \quad (1)$$

$$\sigma_{wall} \ll \frac{K_{1c}}{\sqrt{\pi a}} \quad (2)$$

$$m_1 = 2\pi r^3 P \frac{\rho}{\sigma_y} \quad (3)$$

$$m_2 = 2\pi r^3 P \sqrt{\pi a} \frac{\rho}{K_{1c}} \quad (4)$$

$$M_1 = \frac{\rho}{\sigma_y} \quad (5)$$

$$M_2 = \frac{\rho}{K_{1c}} \quad (6)$$

$$M_1 = C_c M_2 \quad (7)$$

$$C_c = \sqrt{\pi a} \quad (8)$$

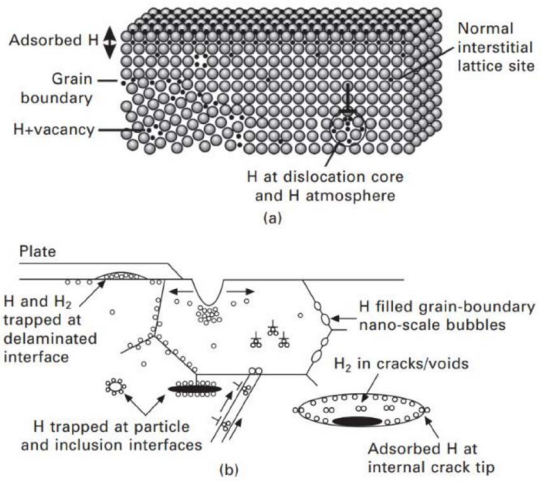

Figure 1: Schematic illustrations of sites and traps for hydrogen in materials (a) on the atomic scale, and (b) on a microscopic scale. Retrieved from: Metallographic and fractographic techniques for characterizing and understanding hydrogen-assisted cracking of metals. DOI: 10.1533/9780857093899.2.274.

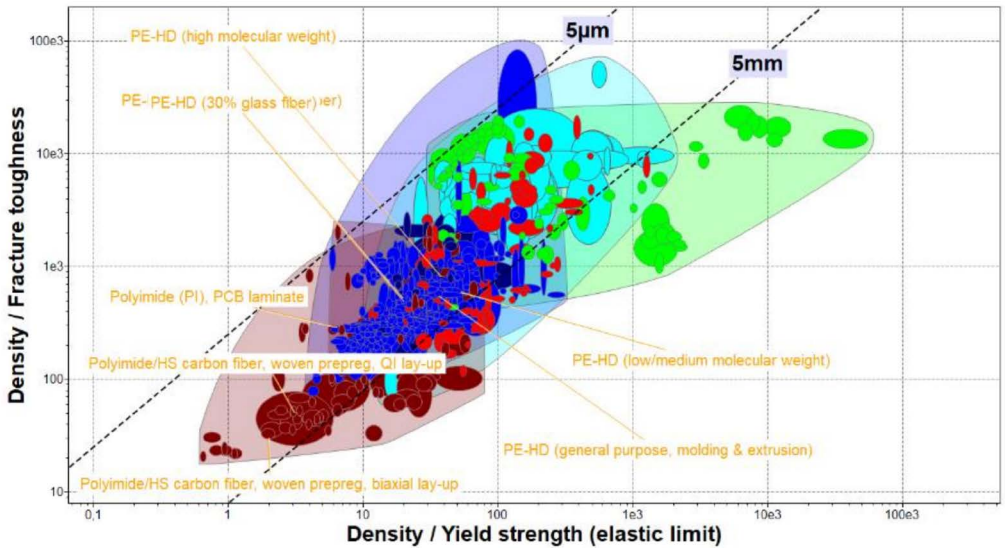

Figure 2: Granta EduPack candidate materials for crack sizes between 5 microns and 5 millimeters.

Development of modular homes for emergency support after natural disasters

Universidade Estadual de Campinas, Brasil

Supervisor: Josué Labaki Silva, PhD

Students: Arthur Mello Marra da Silva, Enzo Vitor Nicoletti, and Fabiane Camargo Carneiro Marinheiro

Contents

1. Summary

Natural disasters, which are increasingly frequent due to climate change factors [1], significantly impact our reality. According to the National Confederation of Municipalities in Brazil [2], floods that occurred in the first half of 2024, in the state of Rio Grande do Sul, Brazil, caused material damage of approximately 1,764,260.00 USD, affecting 106.5 million homes. Additionally, following Hurricane Katrina in New Orleans, USA, in 2005, the city's population shrank by 20% due to 100,000 residents leaving because they no longer had housing [3].

A viable alternative for the countless displaced individuals is the use of modular homes. These homes offer advantages in disaster situations as they are compact, adaptable, and can be quickly assembled and transported [4].

To seek efficient materials for modular homes, the Ansys Granta EduPack software was implemented in the project, providing access to a wide range of materials. It allows the creation and analysis of Ashby diagrams, enabling the identification of essential parameters and the selection of the most appropriate materials for the project.

2. Objectives

With the aid of Ansys Granta EduPack software, the project aims to utilize its various features to develop a modular home capable of sheltering those displaced by natural disasters, under different temperature and humidity conditions, ensuring that access to housing in emergencies is simplified. Thus, the project seeks to select a material that is lightweight yet durable, with a long lifecycle, and features low thermal and electrical conductivity.

3. Problem statement

In a disaster scenario, ensuring assistance for victims is of utmost importance, not only for the

resumption of daily life for those affected but also for the rapid reconstruction of the community. In this regard, modular homes emerge as a viable medium- to long-term solution for the homeless resulting from environmental disasters. Their structure is designed to be modular, allowing for customization and adaptations as needed, while also ensuring ease of transport and assembly. The swift and efficient construction enables the establishment of a significant number of housing units in a short period, greatly enhancing the capacity to address these urgent needs.

The selection of materials for these homes is a crucial factor, reflecting a commitment to versatility and functionality. Therefore, it is essential that the materials used are compatible with the parameters established under the specified conditions and that they meet the planned comfort requirements. Additionally, these materials must possess high quality, ensuring that the structure fulfills expectations in terms of durability and performance.

4. Proposed solution

The selected geometry was gantry. This disposition allows for a light yet robust structure, with patterned pieces, simplifying construction and easing transportation. It's an efficient system that presents good resistance to both vertical and horizontal loads, with the former being its main drawback. To counteract this wind bracing structures are required such as metallic tape in an "X" shape bound to the structure's diagonals [5] (Figure 1). Besides that, the gantry structure may have its pieces easily bound by a self-connecting system, locking the structure in all directions guaranteeing more rigidity [6] (Figure 2).

For the home's insulation a sandwich panel wall was chosen to optimize each of the materials' properties. The core's material was selected with the goal of providing electrical and thermal insulation to the structure. As a thermal parameter it was considered the UNHRC's (The UN Refugee Agency) recommendation of utilizing the cold environment's specifications when designing shelter for different climates. Therefore, considering materials used in structures in the arctic [7] a maximum conductivity of 0.04 W/mK was chosen.

The limit selected for the electrical conductivity was 0,00033 $\Omega^{-1}m^{-1}$, value taken from concrete [8] as structures with this material frequently deal with electrical discharges in urban environments. With these parameters a graph was plotted (Figure 3) minimizing density, cost and thermal conductivity (II and IV), leading to the selection of PP foam. The materials excellent behavior in water (Figure 4) solidified the results.

Selecting materials for the external layers considered the capacity of the material supporting tension, being tough and light. The required tension was calculated based on the wind loads(I) the house would bear. The result was used in Engineering Solver to simulate a minimum Young's modulus of 133 GPa (Figure 5) for the material. This value was used to plot a graph relating toughness with density and price (Figure 6) which highlighted 2 groups for selection: steels and composites. Between them composites were selected given their lower density and higher corrosion resistance, with epoxy carbon being chosen.

For the selection of the gantry's material a model was created (Figure 7) based on other modular home structures [9]. The floor is 5x8m giving an area of 40m^2 which can house up to 5 people comfortably (Figure 8). The roof goes from 2.5 to 3m, creating an incline which prevents the accumulation of water and debris. For the supporting beams a 150x150mm square profile was chosen for the external structure and 120x120mm on the internal one. Besides that, windows were positioned to guarantee good air flow and the presence of natural light.

To guarantee the structure's viability the weight of the panels was calculated based upon the chosen materials' densities (IV, V, VI) and a load of 1.5 kN/m^2 was applied in accordance with the Brazilian norm ABNT NBR 6120. Placing those values on Ansys Mechanical (Figure 9) showed a bigger deformation on

the floor. Thus, using Engineering Solver on the floor beams resulted in a minimum value of 10.9 GPa (Figure 10). This value was then used in Ansys Granta material selector to identify the best material. Minimizing density (Figure 11), wood was shown to be the most viable, with Spruce (*Picea engelmannii*) being chosen.

The house's foundation must be of swift implementation, high efficiency and low cost. Thus, a structure with metal pillars that can adapt to different topography [10] fixed by concrete blocks was chosen. This foundation adds resistance to horizontal forces such as wind and earthquakes and prevents contact with humid soil.

5. Results and conclusions

The Ansys Granta EduPack software was essential in all the analyses performed, providing a comprehensive overview of the project and offering the necessary tools to filter the assigned specifications. For the project's boundary conditions, several variables were considered, including thermal conductivity, resistivity, cost, water absorption resistance, and hardness. Based on these considerations, the best alternative for the framework structure was identified as Engelmann spruce (Picea engelmannii), with its density supporting the choice. For the internal material of the house, polypropylene foam (PP foam) was selected, while the optimal materials identified for the external panel were stainless steel and epoxy carbon.

In the final selection of an external material for the house, the Granta diagrams were analyzed, and epoxy carbon emerged as the best option. This is because it proved to be as lightweight and strong as the other alternatives, with the added advantage of being non-corrosive. Furthermore, the cost-benefit analysis demonstrated it to be the most favorable among the materials considered, making it the chosen material for the modular home's panels.

6. References

[1] Nations, U. (n.d.). *Causas e Efeitos das Mudanças Climáticas* | Nações Unidas. [online] United Nations. Available at: https://www.un.org/pt/climatechange/science/causes-effects-climate-change.

[2] Confederação Nacional de Municípios. (2024) *Prejuízos com as chuvas no Rio Grande do Sul passam de R$ 10 bilhões.* [online] Available at: https://cnm.org.br/comunicacao/noticias/

[3]G1. (2024). *Destruída por inundações do furacão Katrina*, Nova Orleans traz lições de reconstrução para o RS. [online] Available at: https://g1.globo.com/fantastico/noticia/2024/05/12/

[4] Mendes, R. C., & Barbosa, L. L. *Documentação de imagens referentes aos sistemas e componentes para design modular em situações de desastres.*

[5] UFMT. CONTRAVENTAMENTOS. (n.d.). [online] Available at: https://organizacaotc.wordpress.com/wp-content/uploads/2014/04/telhados03.pdf

[6] Griz, C., Nome, C. and Queiroz, N. (n.d.). *Edificação Modular: Estudo de caso e protótipo de um sistema construtivo de código aberto utilizando prototipagem rápida*. [online] Available at: http://dx.doi.org/10.5151/sigradi2017-042

[7] UMNYAKOVA, N. et al. Arctic Climate Insulation Systems. MATEC Web of Conferences, v. 298, p. 00012, 2019.

[8] MELO, L.; SILVA, A. Universidade Federal de Goiás Escola de Engenharia Civil e Ambiental Curso de Graduação em Engenharia Civil Resistividade Elétrica Superficial do Concreto: Influência da Cura. [s.l: s.n.]. Available at:: < http://repositorio.bc.ufg.br/handle/ri/11303f>

[9] MIGUEL, F.; FREITAS, C. [s.l: s.n.]. Available at: <https://core.ac.uk/download/pdf/148828408.pdf>.

[10]Salviano, H.C., 2016. *NHABE-Núcleo Habitacional Embrionário: Habitação intermediária para famílias vítimas de desastres naturais*. Trabalho de Graduação. Universidade Federal do Rio

Grande do Norte, Natal.. Available at: <https://repositorio.ufrn.br/bitstream/123456789/36722/9/HabitacaoVitimasDesastresNaturais_Salviano_2016.pdf>

7. Appendix

Variables Used		Equations and solutions
$\rho_a = 1.2041\ kg/m^3$	Air density at 20ºC and 1 atmosphere of pressure	I) $F = \frac{1}{2}\rho v^2 A C_d$; $F = 15701.25kN = 15700kN$
$v = 19{,}7\ m/s$	Wind speed selected to be within category 8 of the Beaufort scale	II) $M_1 = \frac{1}{\lambda \rho C_m}$; Minimize M_1
$A_o = 64\ m^2$	Area of the overdimensioned home as a 8m sided cube	III) $M_2 = \frac{\varphi}{\rho C_m}$; Minimize M_2
C_d = 1,05	Drag coefficient for a cube	IV) $W\ pp = A\ .\ \rho_{pp}.T_{pp}$; $W\ pp$ = 5.7 kN $W\ pp$ being the weight of the PP foam ρ_{pp} being the density of PP foam T_{pp} being the thickness of PP foam in each panel
λ	Thermal conductivity	V) $W\ c = A\ .\ \rho_C.T_C$; $W\ c$ = 47.36 kN $W\ c$ being the weight of the carbon composite ρ_C being the density of the carbon composite T_C being the thickness of each composite panel
φ	Electrical resistivity	VI) $W = Wpp + Wc$; W the total weight on the house
C_m	Cost factor	ρ_{pp} = 21 Kg/m³; ρ_C = 1.55e3 Kg/m³; T_{pp} = 0.2m; T_C = 25mm

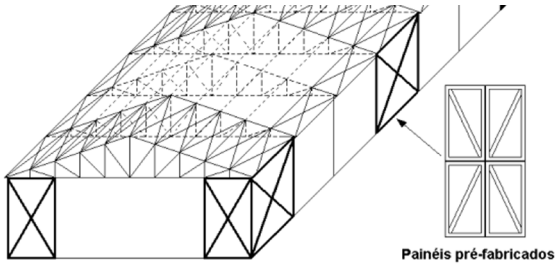

Figure 1: X-shaped wind bracing structure [5].

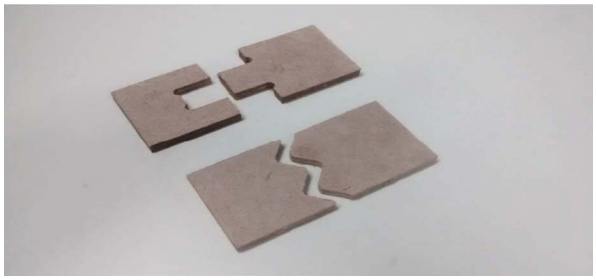

Figure 2: Example of self connecting pictures [6].

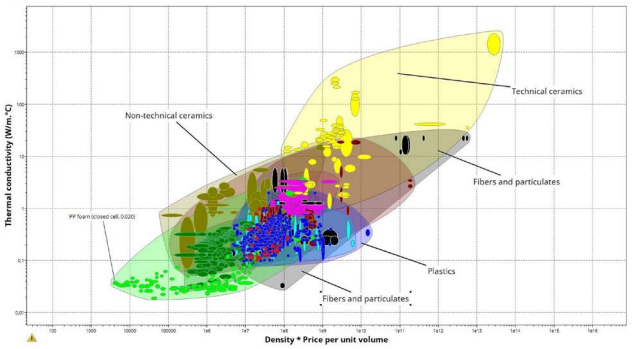

Figure 3: Thermal conductivity versus density graph, considering thermal conductivity and cost,the green bubble symbolizing materials that meet the minimum requirements: Authorial.

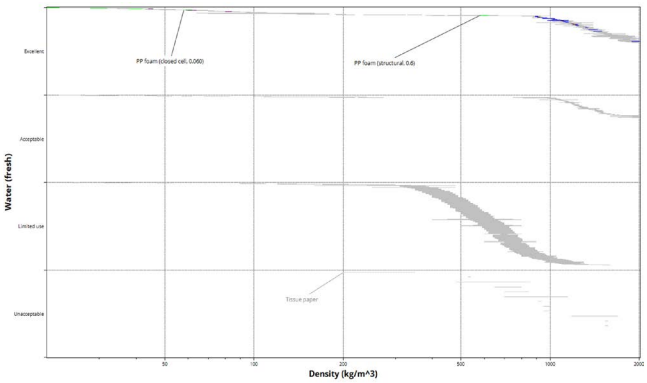

Figure 4: Fresh water versus density graph, PP foam has little absorption: Authorial

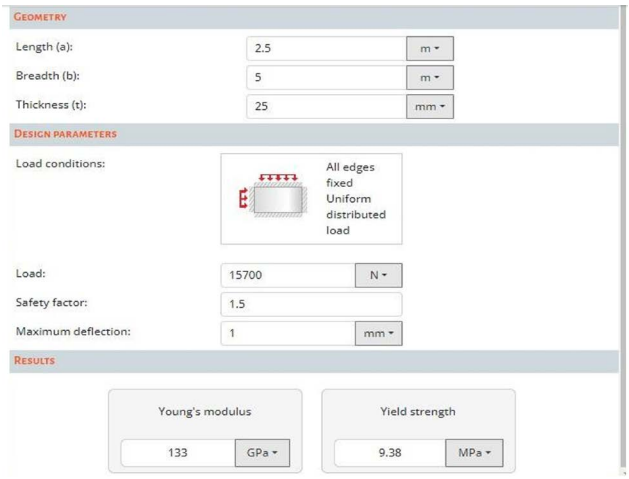

Figure 5: Ansys Granta Solver solution for the required Young's modulus for the external wall panels: Authorial.

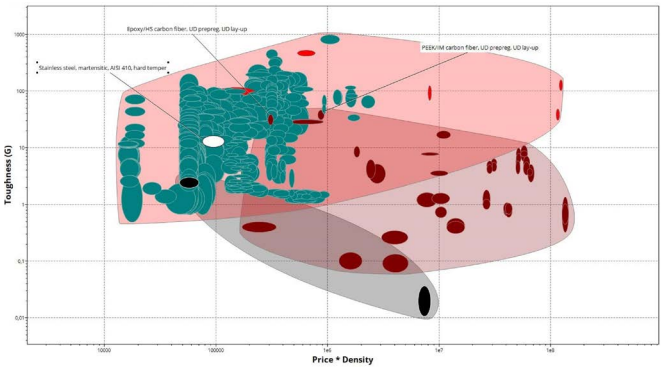

Figure 6: Toughness versus density graph, considering cost highlighting epoxy carbon fiber composite against other considered materials: Authorial

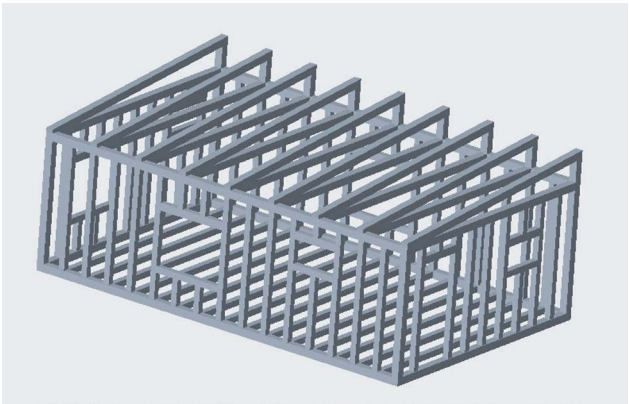

Figure 7: 3D model of the gantry home structure: Authorial

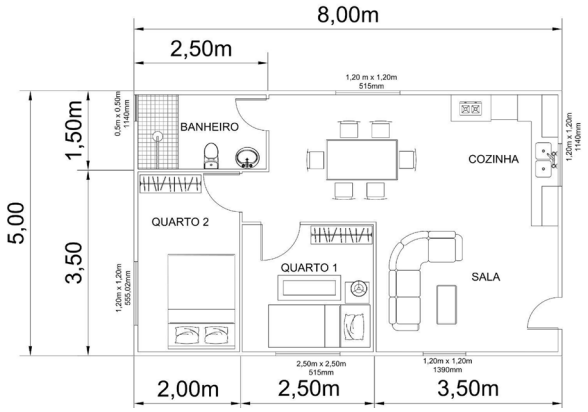

Figure 8: Blueprint suggestion for the internal disposition of the modular home: Authorial

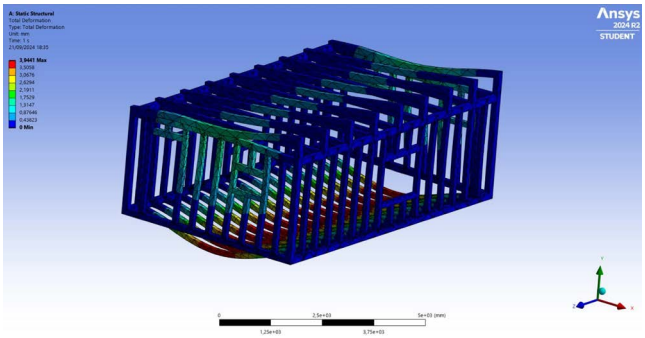

Figure 9: Static simulation of the house model using Ansys Mechanical solving for deformation. Biggest deformation found on the floor: Authorial.

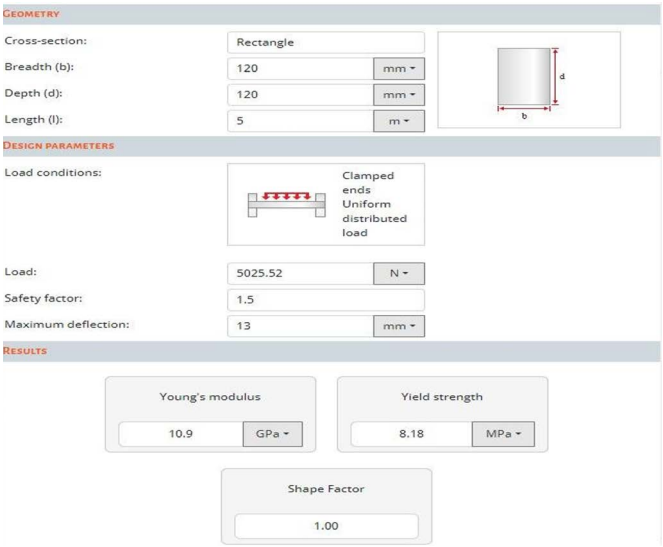

Figure 10: Ansys Granta Solver solution for the required Young's modulus for the structure's beams: Authorial.

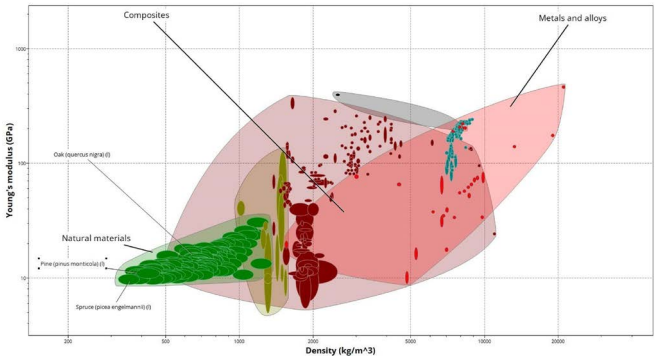

Figure 11: Density versus Young's modulus graph with the green bubble indicating the lower density natural materials. The selected wood Picea engelmannii is highlighted: Authoral.

Figure 12: Variable height foundation [11].

Material selection for the *Liedna*: A traditional Maltese village feast decoration

University of Malta, Msida, Malta

Supervisor: Dr Inġ. Anthea Agius Anastasi & Dr Sophie M Briffa

Students: Shana N'Douri Sangana

Contents

1. Summary

The celebration of traditional Maltese village feasts dates to the 18th century under the rule of the Knights of St. John [1]. These annual religious *festas*, recognised by UNESCO Intangible Cultural Heritage [2], are deeply embedded in Catholic tradition and community identity. They pay tribute to the village's patron saint and showcase the local devotion and religious heritage. The feasts are a vibrant amalgamation of faith, tradition, and community spirit, bringing together both locals and visitors. Festivities typically include lively processions featuring statues of the saints, band marches, firework displays, decorative lights, church services, and traditional Maltese food, drinks and sweets. Beyond their religious significance, these feasts serve as important social events that foster community pride, strengthen local bonds, and preserve Malta's rich cultural traditions. In preparation for these celebrations, streets are enthusiastically adorned. A notable decoration used during this time is the "liedna," or garland (see Figure 1a). To this day, the *liedna* is handmade by local volunteers by tying a series of brightly coloured rectangular sheets of plastic around a rope using simple knots. However, with repeated use, the materials of the *liedna* deteriorate and contribute to significant plastic pollution, with small plastic fragments littering the streets (see Figure 1b), necessitating volutneers to prepare new *liedna* every few years. The aim of this study was to carry out a material selection process to identify a more eco-friendly and durable alternative material for the *liedna*. Through a material selection process using Ansys Granta EduPack, several natural materials were identified as viable options, which are now undergoing a UV exposure study.

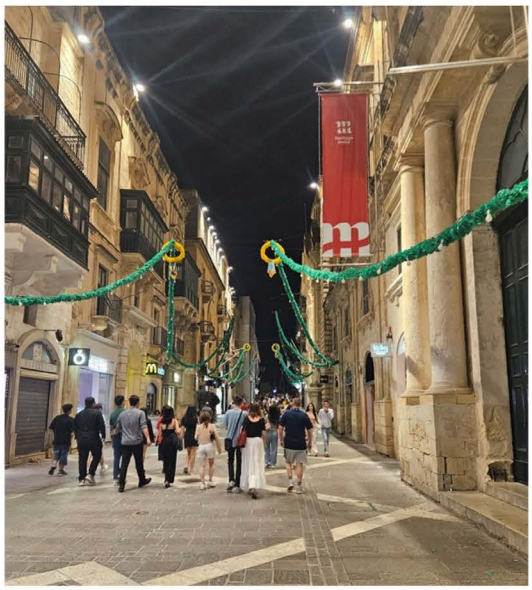

(a)

(b)

Figure 1: (a) Maltese liedna decorating the streets for the village feast, and (b) degraded liedna littering the street.

2. Objectives

The overall aim of this study was to identify a more eco-friendly and durable alternative material for the *liedna*. The following objectives were identified:

1. To characterise the current material used for the *liedna* decoration and understand the material requirements for such decoration.
2. To use Ansys Granta EduPack to select a number of alternative materials that could be used for the *liedna*. Such materials need to offer an eco-friendlier solution.
3. To prepare prototypes using the suggested materials and run experiments to determine the durability of the materials under UV exposure.

For the purpose of this report and challenge, Objective 2 alone will be focused on .

3. Problem statement

The traditional *liedna* decorations utilised during village feasts in Malta pose significant environmental challenges due to their contribution to plastic pollution, as evidenced by the presence of plastic fragments on the streets following each event (Figure 1b). Furthermore, these decorations have a limited lifespan, requiring replacement every 4 to 5 years due to colour loss and material degradation, which exacerbates waste generation and adversely affects the environment. The recurrent need for replacement and disposal underscores the critical necessity for developing more sustainable alternatives that can mitigate plastic pollution and promote environmental responsibility in celebratory practices. In response, the University of Malta was commissioned by Hon. Dr Owen Bonnici MP on behalf of the Ministry for the National Heritage, the Arts and Local Government of Malta to identify a more durable and eco-friendly material that can replace the current materials used for the *liedna* and in turn reduce plastic waste and pollution.

4. Proposed solution

The study was carried out in Level 3 Sustainability of the materials universe in Ansys Granta EduPack

2020 due to its large selection of sustainable materials. During this process, the reference material for comparison was set to low-density polyethylene (LDPE), the material which is currently used for the Maltese *liedna* as evidenced by characterisation and research carried out previously to satisfy Objective 1 of this study. As part of Objective 1, a set of requirements that the material needs to satisfy was also compiled following consultation with local *liedna* artisans and is shown in Appendix 1. It was determined that an increase in cost might be justified if the material is more durable, sustainable, and eco-friendly. The material selection process was carried out in two stages. A global approach was first used in which many aspects and materials were considered. The second approach was based on a classification of the materials in the database. Details for both are given below.

Global Approach

This approach was initiated by eliminating as many materials as possible with a limit step containing the established requirements in Appendix 2, such as maximum service temperature, resistance to water and UV radiation, and biodegrability. Material comparisons were then made based on four other criteria, presented in Appendix 3 – water usage (L/kg) (Criterion 1), the CO_2 footprint of primary production (kg/kg) (Criterion 2), the absorption of saturated water (%) (Criterion 3), and the performance index $E^{(1/3)}/(\rho C_m)$ (Criterion 4) derived in Appendix 4 [3].

Natural Material Focused Approach

This approach was carried out after identifying the critical criteria of biodegradability, recyclability, and flammability, with the materials possibly falling under either of the four classifications outlined in Table 1. It was noted that a material cannot be both biodegradable and recyclable with current recycling facilities available in Malta.

Table 1 Classification of materials.

	Biodegradability	Recyclability
Non-flammable	Biodegradable (B)	Recyclable (R)
Highly flammable	Biodegradable and flammable (BF)	Recyclable and flammable (RF)

For the *liedna*, the material is ideally biodegradable and non-flammable (Case B), and of natural origin, so that any deteriorated material littering the streets would have a lower impact on the environment. To minimise the *liedna's* impact, it is preferable that the material also has the lowest possible carbon footprint. Currently, neither the *liedna* nor the debris is recycled because the material is too degraded by the end of its life. Choosing a biodegradable material could address this problem. As such, focus was placed on natural materials, possibly considering the biodegradable and flammable materials (Case BF). The database from which the materials were selected was modified as follows:

1. "Natural fibres" was selected from the Fibres and Particulate database
2. "Wood-like materials" was selected from the Hybrid database
3. "Thermoplastic" was selected from the Polymers database to allow comparison with the LDPE

5. Results and conclusions

Results from the Global Approach

The first approach only identified general-purpose and flame retarded polylactic acid (PLA) as alternative materials that passed all the criteria specified in Appendix 2 and 3 and performed as well as, or better than, LDPE. Table 2 presents the identified properties used to compare the three materials. Out of the

three materials, general-purpose PLA is the least water-consuming in the primary production phase. Furthermore, while LDPE performs the best in the other properties identified, exhibiting the lowest carbon footprint, lowest cost, and lowest 24-hour water absorption, both PLAs are still deemed to be competitive upon considering the performance index (Criterion 4). It is noted that, although the 24-hour water absorption values give an indication of the ease with which materials absorb water/ moisture, they do not allow to validate, or otherwise, the suitability of a material in this application since no threshold value has been identified.

Table 2 Identified material properties of general-purpose PLA, flame retarded PLA, and LDPE.

	Water Consumption (L/kg)	Carbon Footprint (kg/kg)	Price (€/kg)	24-hour Water Absorption (%)
LDPE	72 - 79.6	**1.79 - 1.98**	**1.02 - 1.27**	**0.005 - 0.01**
General-purpose PLA	**19.8 - 21.8**	2.7 - 2.98	1.99 - 3.36	0.24-0.26
Flame retarded PLA	1250 - 1380	3.19 - 3.52	2.81 - 4.21	0.12-0.13

Results from the Natural Material Focused Approach

The approach focusing on natural materials resulted in a different set of promising material alternatives. When considering biodegradable and non-flammable materials (Case B, Appendix 5), cork was identified as an alternative although it has a greater water consumption (665-735 L/kg) than LDPE, even though cork is a natural material. Cork is also more expensive than LDPE at 2.4 - 12 €/kg. However, the performance index validates the competitiveness of cork. The carbon footprint of cork (0.192 – 0.211 kg/kg) is also much lower than that of LDPE. Furthermore, while the water absorption of cork at 24 hours was not found, cork is known to resist rotting [4] and therefore should meet the humidity criterion. The lack of flexibility of the cork could lead to tearing during the manufacture of the *liedna*. To circumvent this, use of cork fabric could be a solution.

Upon considering the biodegradable but flammable materials (Case BF, Appendix 6), several natural materials were identified. Overall, their water consumption was found to be around three times higher than that of LDPE. However, their carbon footprint was similar or lower than that of LDPE. Kenaf, jute, and coconut fibres, and palm where the materials that performed better than LDPE in the performance index considered.

As such, the material selection process using Ansys Granta EduPack resulted in PLA, cork, kenaf, jute, and coconut fibres, and palm to be considered as alternative materials for the *liedna*. However, it was noted that one of the most important criterions considered, which was the UV durability given that the *liedna* is exposed to a high UV climate during Maltese summers, is only qualitative in the Ansys Granta EduPack database and it is based on an estimate of the years during which a material can withstand UV exposure. In fact, in the results shown in Appendix 6, cotton appears to be an interesting material however does not pass the UV durability criterion set earlier. To investigate whether cotton would indeed be a promising material, and especially considering its ease of purchasing and colouring with bright colours unlike the rest of the natural fibres, a criterion which could not be considered in the material selection software but essential for brightly coloured decorations, four textiles made of cotton, canvas, polyester and jute were purchased from a local shop. Samples in preparation for tensile testing as per ISO 13934-1 and ISO 527-were prepared out of all four materials and also the LDPE currently used in the *liedna* and were exposed to UV irradiation in a custom-built aging chamber [5] with an irradiance of 302 Wm^2 and UV-A irradiance of 18.7 Wm^2. The UV aging study is ongoing but following exposure for 1 week, 2 weeks and 4 weeks, the mechanical behaviour and the colour change

will be analysed.

6. References

[1] Cassar, C. (2006). The Maltese Festa: A Historical and Cultural Perspective. In G. Mifsud-Chircop (Ed.). The First International Conference of the SIEF on The Ritual Year: Proceedings (45-87). Malta: PEG.

[2] UNESCO - Decision of the Intergovernmental Committee: 18.COM 8.B.43 (2023) UNESCO Intangible Cultural Heritage. Available at: https://ich.unesco.org/en/decisions/18.COM/8.B.43 (Accessed: 31 August 2024).

[3] M. F. Ashby, Materials selection in mechanical design. Oxford ; Burlington (Mass.): Elsevier, 2011.

[4] A. Mestre, and L. Gil, "Cork for sustainable product design" In: Ciência e Tecnologia dos Materiais, 2011, vol. 23, nº 3-4, p. 52-63

[5] J. Galea, A. Agius Anastasi, and S. M. Briffa, "Design of a Weathering Chamber for UV Aging of Microplastics in the Mediterranean Region," *ACS Omega*, Aug. 2024, doi: https://doi.org/10.1021/acsomega.4c03735.

7. Appendix

Appendix 1: Table of Material Requirements

Criterion	Function Name	Description	Flexibility Index
Environmental			
E1	Heat resistance	Withstand prolonged exposure at 50°C	0
E2	UV resistance	Resist Malta's maximum UV index of 11	0
E3	Cleaning	Be cleaned easily	0
E4	Dust	Does not collect dust easily	2
E5	Resistance urban pollution	Not weakened by car pollution	1
E6	Water resistance	Does not degrade or change shape when in contact with rain water or sea spray	0
E7	Resist humidity	Does not rot in humid storage spaces	0
E8	Flammability	Non flammable	2
Visual			
V1	Colouring	Able to be coloured to bright colours (blue, red, yellow, green)	0
V2	Shape	Stiff enough to hold its full shape when tied to the main rope	0
Ecological			
EC1	Durability	Usable for at least 5 years	0
EC2 EC2a EC2b EC2c EC2d	Respect for the environment	Minimise the impact of the material used on the environment throughout its life cycle: - Use a local material - Use a natural material - Use a biodegradable material - Use a recyclable material	0 2 1 1 1

Appendix 2: Limits Criteria

Stage	Attribute	Constraints
1	Maximum service temperature (°C)	≥ 50
	Contains >5wt% critical elements?	No
	Water (fresh)	Limited use, Acceptable, Excellent
	Water (salt	Limited use, Acceptable, Excellent
	UV radiation (sunlight)	Good, Excellent
	Flammability	Slow-burning, Self-extinguishing, Non-flammable
	Recycle	✓
	Biodegrade	✓

Appendix 3: Global Approach - Material Comparison Charts

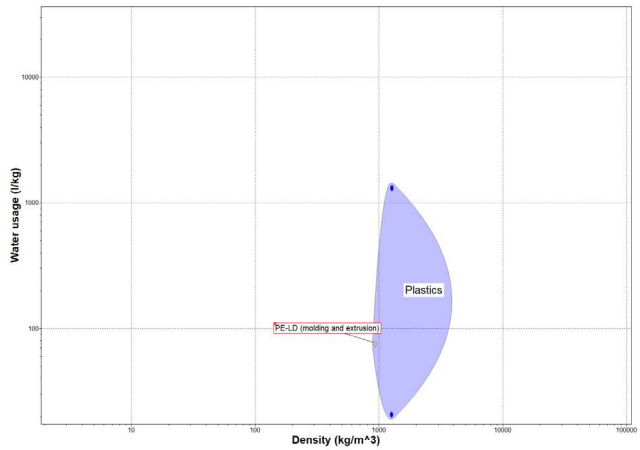

Criterion 1

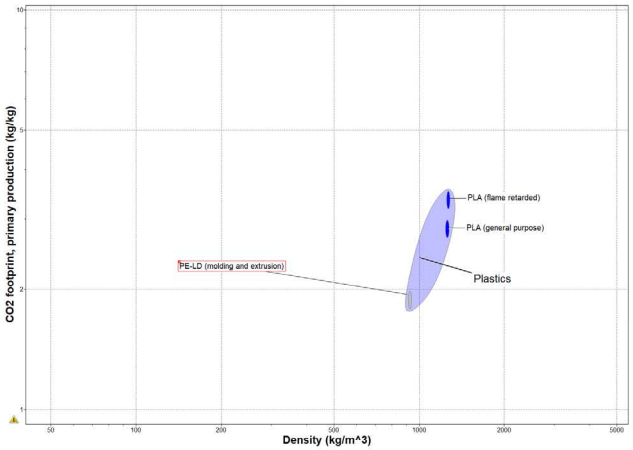

Criterion 2

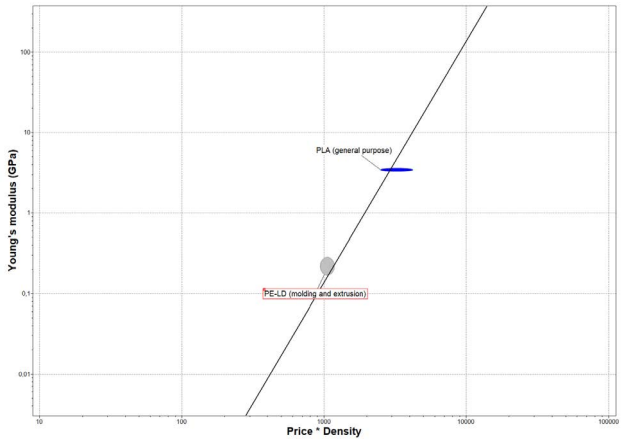

Criterion 4

Appendix 4: Performance Index Derivation

Criterion 4 was based on performance index, *P* [3]. Equation 1 details the price of one rectangular sheet that makes up the *liedna, C*, as a function of its material price per kilo, C_m, geometric parameters, *b*, *h*, and *L*, material density, *ρ*.

$$C = bhL\rho C_m \quad (1)$$

Equation 2 shows the bending stiffness, *S*, that the *liedna* sheet must satisfy (at least S^*) so that it does not break when tightening the knot upon preparation of the *liedna*. C_1 is a constant, and *E* is the elastic modulus.

$$S = \frac{C_1 E}{L^3}\left(\frac{bh^3}{12}\right) \geq S^* \tag{2}$$

By combining these equations, Equation 3 and the associated performance index in Equation 4 are obtained.

$$C = \left(\frac{12S^*}{C_1 b}\right)^{\frac{1}{3}} (bL^2)\left(\frac{\rho C_m}{E^{\frac{1}{3}}}\right) \tag{3}$$

$$P = \frac{E^{\frac{1}{3}}}{\rho C_m} \tag{4}$$

Equation 5 was then used on Ansys Granta EduPack to plot E against ρC_m. A selection guide line with a slope of 3 was then drawn and the materials falling above the selection line were considered to perform better.

$$\log E = 3 \log P + 3 \log(\rho C_m) \tag{5}$$

Appendix 5: Natural Materials Focused Approach: Material Comparison Charts for Case B

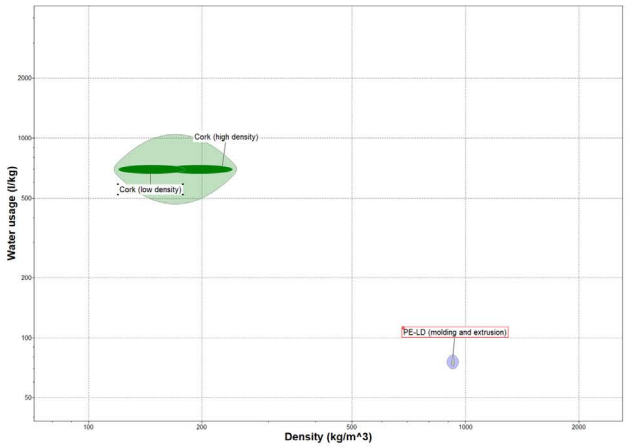

Criterion 1

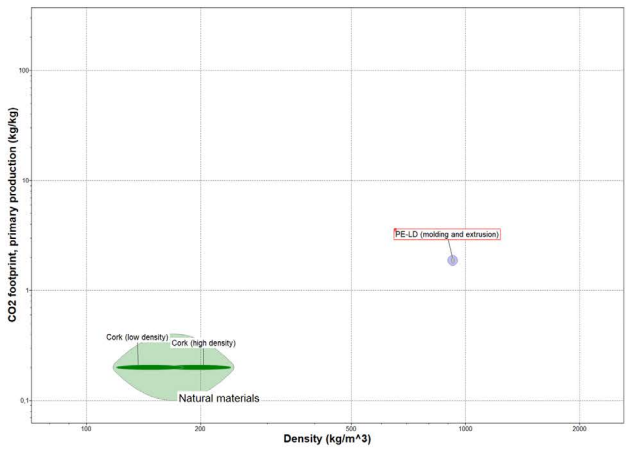

Criterion 2

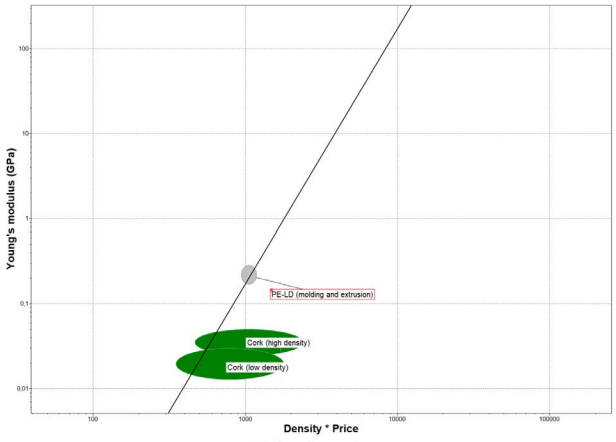

Criterion 4

Appendix 6 : Natural Materials Focused Approach: Material Comparison Charts for Case BF

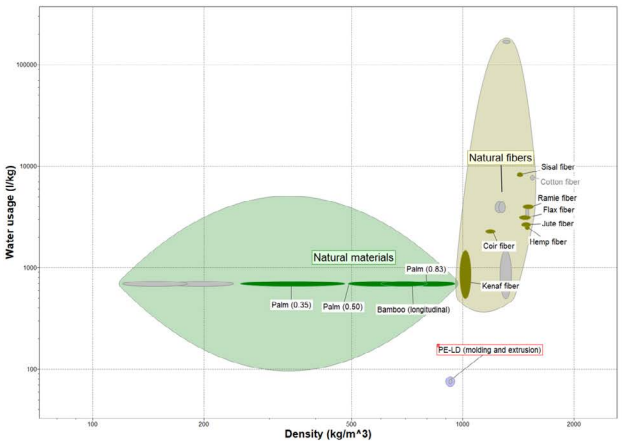

Criterion 1

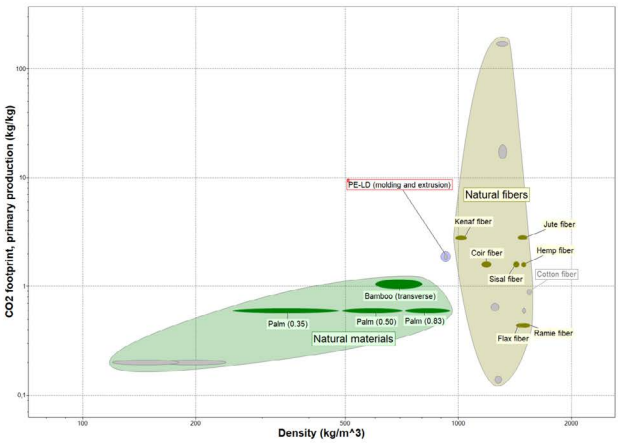

Criterion 2

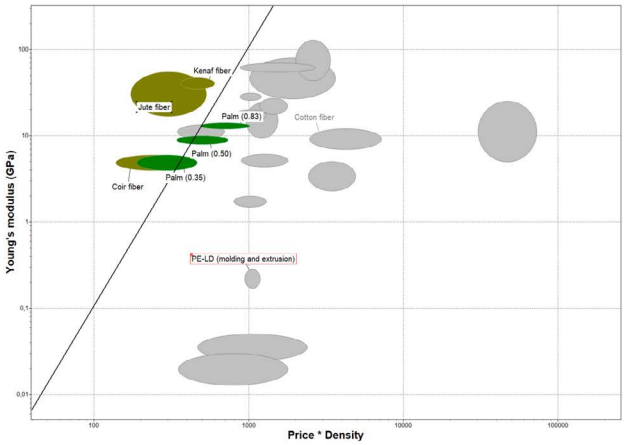

Criterion 4

Use and Reproduction

The content used in this resource may only be used or reproduced for teaching purposes; and any commercial use is strictly prohibited.

Document Information

This case study is part of a set of teaching resources to help introduce students to multiphysics topics.

Ansys Education Resources

To access more undergraduate education resources, including lecture presentations with notes, exercises with worked solutions, MicroProjects, real life examples and more, visit www.ansys.com/education-resources.

Feedback

Here at Ansys, we rely on your feedback to ensure the educational content we create is up-to-date and fits your teaching needs.

Please click the link here out a short survey (~7 minutes) to help us continue to support academics around the world utilizing Ansys tools in the classroom.

ANSYS, Inc.
Southepointe
2600 Ansys Drive
Canonsburg, PA 15317
U.S.A.
724.746.3304
ansysinfo@ansys.com